EMIn-depth profiling of calcite precipitation by environmental bacteria reveals fundamental mechanistic differences with relevance to application

Bianca J. Reeksting[1], Timothy D. Hoffmann[1], Linzhen Tan[2], Kevin Paine[2] and Susanne Gebhard[1]*

[1]Department of Biology and Biochemistry, Milner Centre for Evolution, and [2] BRE Centre for Innovative Construction Materials, University of Bath, Claverton Down, Bath, BA2 7AY, United Kingdom

Running title: Calcite precipitation by environmental bacteria

Key words: ureolysis, self-healing concrete, microbial-induced calcite precipitation, *Bacillus*

*Author for correspondence. Tel: +44 (0) 1225-386421 Email: s.gebhard@bath.ac.uk

SUMMARY

Microbial-induced calcite precipitation (MICP) has not only helped to shape our planet's geological features, but is also a promising technology to address environmental concerns in civil engineering applications. However, limited understanding of the biomineralization capacity of environmental bacteria impedes application. We therefore surveyed the environment for different mechanisms of precipitation across bacteria. The most fundamental difference was ureolytic ability, where urease-positive bacteria caused rapid, widespread increases in pH, while non-ureolytic strains produced such changes slowly and locally. These pH shifts correlated well with patterns of precipitation on solid media. Strikingly, while both mechanisms led to high levels of precipitation, we observed clear differences in the precipitate. Ureolytic bacteria produced homogenous, inorganic fine crystals, whereas the crystals of non-ureolytic strains were larger with a mixed organic/inorganic composition. When representative strains were tested in application for crack healing in cement mortars, non-ureolytic bacteria gave robust results, while ureolytic strains showed more variation. This may be explained by our observation that urease activity varied between growth conditions, or by the different nature and therefore material performance of the precipitate. Our results shed light on the breadth of biomineralization activity among environmental bacteria, an important step towards the rational design of bacteria-based engineering solutions.

INTRODUCTION

Environmental protests worldwide have highlighted a growing demand for action on the threat of climate change. Human activity has greatly contributed to global warming, currently causing an estimated 0.2°C increase per decade due to past and ongoing emissions (Intergovernmental panel on climate change (IPCC) 2018 report). There is a clear need to reduce our carbon dioxide (CO_2) emissions as well as to find novel ways in which we can consume CO_2 as a means of decreasing overall levels. Geological sequestration of CO_2 from large point source emitters into carbonate minerals, such as dolomite and limestone, is an emerging technology that could mitigate increasing CO_2 concentrations (Mitchell *et al.*, 2010). Microorganisms can act as biomediators to enhance carbon capture (Mitchell *et al.*, 2010) by microbial induced calcite precipitation (MICP). This process leads to precipitation of CO_2 as calcium carbonate ($CaCO_3$) as a result of microbial metabolism and has been occurring on a geological scale for more than 2.5 billion years (Altermann *et al.*, 2006). The formation by microbes of mineral carbonate structures, termed microbialites, is mediated by a large diversity of microorganisms, often working together in a consortium (Wilmeth *et al.*, 2018). Indeed, cyanobacteria in association with heterotrophic bacteria are thought to be the principal contributors to the production of carbonate rocks during almost 70% of Earth's history (3.5-0.5 Ga) (Altermann *et al.*, 2006).

The success of MICP in biological engineering of the environment has led to the investigation of its potential for exploitation in other areas. These areas include bioremediation of heavy-metal contaminated soils via immobilisation of metals in precipitates (Achal *et al.*, 2011; Ceci *et al.*, 2018), or wastewater treatment using this technology to remove excess calcium. Geotechnical engineering represents another area of interest, where MICP can improve soil properties by precipitating $CaCO_3$ to bind sand particles together. Utilizing MICP in the construction industry is another rapidly emerging field. The production and maintenance of concrete bears heavy environmental and economic costs, with cement production contributing up to 5-8 % of global anthropogenic CO_2 emissions

(Huntzinger and Eatmon, 2009; Souto-Martinez *et al.*, 2018). Moreover, reinforced concrete structures face durability issues caused by cracking and subsequent ingress of water and ions, such as chlorides. This leads to corrosion of internal steel reinforcement and eventual structural failure. MICP can seal such cracks in concrete and reduce permeability to damaging substances, thereby extending the lifespan of structures and reducing the environmental burden caused by construction of replacement structures. This broad range of applications necessitates an understanding of how bacteria precipitate calcite and what the factors are that may limit their performance.

Most bacteria are capable of MICP under suitable conditions (Boquet *et al.*, 1973), with key factors such as calcium concentration, concentration of dissolved inorganic carbon (DIC), pH, and availability of crystal nucleation sites affecting precipitation (Hammes and Verstraete, 2002). Bacterial metabolism results in an increase in both pH and DIC (through aerobic or anaerobic oxidation of organic compounds), and changes in solution chemistry (Power *et al.*, 2011). This can lead to the oversaturation of Ca^{2+} and CO_3^{2-} ions to facilitate the formation of calcium carbonate precipitates (Power *et al.*, 2011). The negatively charged cell surfaces of bacteria further promote precipitation by attracting calcium ions and acting as nucleation sites for crystal formation (Zhu *et al.*, 2016).

To date, the majority of studies of MICP have focussed on ureolytic bacteria (Zhu *et al.*, 2016). These are associated with high rates of $CaCO_3$ precipitation (Mitchell *et al.*, 2010), caused by hydrolysis of urea ($CO(NH_2)_2$) to ammonia (NH_3) and carbonic acid (H_2CO_3) (Mitchell *et al.*, 2010). The reaction of ammonia with water to ammonium (NH_4^+) and hydroxide ions (OH^-) causes an upshift in pH, while carbonic acid dissociates to generate bicarbonate (HCO_3^-). In the presence of calcium, this leads to the formation of a calcium carbonate ($CaCO_3$) precipitate (Equations 1 and 2).

$$CO(NH_2)_2 + 2H_2O \rightarrow 2NH_4^+ + CO_3^{2-} \quad (1)$$

$$Ca^{2+} + CO_3^{2-} \rightarrow CaCO_3\ (s) \quad (2)$$

Ureolytic MICP has been used in a range of applications. Positive outcomes were obtained in the improvement of soil properties, however non-uniform rates of precipitation throughout the samples led to varying results (Zhao *et al.*, 2014). In addition, the requirement for injection of the healing agent into the ground created problems where the rapid precipitation initiated by urease activity caused clogging at the injection site (Cheng and Cord-Ruwisch, 2014). In other applications, such as crack sealing in cementitious materials, ureolytic MICP has been shown to promote healing (Bang *et al.*, 2010; Wang *et al.*, 2012). However, because of the dependency of the reaction on enzymatic activity, factors such as low temperature markedly decreased the efficiency of the reaction (Wang *et al.*, 2017). In addition, ureolytic MICP requires the presence of urea, which may not always be feasible to provide, and the release of ammonia could contribute to environmental nitrogen loading (Jonkers *et al.*, 2010).

To work around the challenges associated with ureolytic bacteria, the use of other metabolic pathways needs consideration. The high efficiency of ureolytic MICP has resulted in the assumption that non-ureolytic pathways cannot yield similarly high levels of precipitation and are thus an inferior strategy to achieve precipitation. This has limited our understanding of alternative pathways, and the factors affecting efficient calcite precipitation in non-ureolytic bacteria are not clear. Studies on self-healing concrete using alkaliphilic non-ureolytic bacteria, such as *Bacillus pseudofirmus* and *Bacillus cohnii*, have shown great promise and have led to similar levels of self-healing at the laboratory scale as ureolytic bacteria (Sharma *et al.*, 2017; Alazhari *et al.*, 2018). To fully assess the potential of MICP for industrial and environmental use, detailed understanding of the microorganism, mechanism of precipitation, and application is therefore important.

Most studies of MICP have focussed on a small number of species and have thus restricted our understanding of the mechanisms of precipitation across bacteria. In addition, many previous studies have been primarily application-driven and have not always explored the deeper workings of how the bacteria precipitate minerals and what influences this ability. To

115 build a strong basis on which to develop our understanding of MICP, we here took a broad
116 view and surveyed in detail the ability of environmental bacteria to precipitate calcite.
117 Focussing on bacteria that could grow in the alkaline conditions typical of high-calcium
118 environments, we assessed the prevalence of MICP capability in environmental bacteria,
119 their mechanisms of precipitation and resulting crystal morphologies as well as their
120 suitability for application in self-healing concrete. Our study provides an understanding of the
121 environmental potential for MICP, which is not only relevant to geomicrobiology but will
122 facilitate a more design-based approach to industrial application of MICP.

123

124 **RESULTS AND DISCUSSION**

125 **Calcite precipitation ability of environmental isolates**

126 To gain a broader understanding of the capability of bacteria to precipitate calcium
127 carbonate, we first performed a survey of a range of environments. In this, we focussed on
128 sites expected to be calcium-rich, such as exposed limestone, caves and soils in areas with
129 a limestone bedrock within the southwestern United Kingdom. Our isolation strategy targeted
130 spore-forming bacteria, as their stress tolerance makes them more universally useful in
131 potential applications. Moreover, as many of the high-calcium environments are in the
132 alkaline pH range, we specifically sought for isolates that tolerate such conditions.
133 Interestingly, the majority (89 %) of colonies obtained during primary isolations had visible
134 crystal formation on the surface, indicative of biomineralization. This supports previous
135 observations that this is a common trait among bacteria (Boquet *et al.*, 1973). Of 74 isolates
136 able to grow at pH 9, 31 displayed some growth at pH 10 on 0.25x B4 minimal medium and
137 were chosen for further characterisation.

138 Preliminary identification based on partial sequencing of the 16S rDNA assigned all of the
139 isolates into Bacillales (Fig. 1). The selection of spore-formers by heat-treatment can
140 account for the prevalence of Bacillales, with most isolates grouping within the *Bacillus*

141 genus. The predominant species represented were *Bacillus licheniformis* and *Bacillus*
142 *muralis*. *Sporosarcina pasteurii* was included in the analyses as it represents the paradigm
143 organism for industrial application of calcite precipitation. Interestingly, five of our isolates
144 grouped within the same clade as *S. pasteurii* (Fig. 1).

145

146 **Mechanistic differences in calcite precipitation between isolates**

147 The isolation strategy, with the exception of looking for alkali-tolerant spore formers, was
148 unbiased for particular metabolic properties of the bacteria. A key feature of many known
149 calcite precipitators is ureolysis, which leads to a rapid pH change in the environment due to
150 the release of ammonia and subsequent production of OH^-. We therefore tested each of our
151 isolates for their ability to cleave urea, which is visible as a pink colour change in test broth
152 containing urea and phenol red (Fig. 2 and Fig. S2). Five out of the 31 isolates taken
153 forward for further characterisation were ureolytic. Two of these ureolytic isolates (CG4_2
154 and CG6_1) were most closely related to *B. muralis* whilst two others (CG7_2 and CG7_3)
155 were identified as *Lysinibacillus fusiformis*. The final isolate (EM1) was identified as
156 *Psychrobacillus psychrodurans* and was most closely related to *S. pasteurii*. With the
157 exception of CG4_2 and CG6_1, the other ureolytic isolates formed a monophyletic clade
158 with the strongly ureolytic *S. pasteurii* (Fig. 1).

159 To determine the effects of ureolysis and the associated pH change on crystal formation, we
160 repeated the experiment on solid media. Non-ureolytic strains showed only small changes in
161 pH, as indicated by local colour changes in the immediate vicinity of the bacterial colony, due
162 to general metabolic activity (Fig. 2, isolate RC1_1; Fig. S2). In contrast, a rapid and wide-
163 spread increase in pH was apparent in the model ureolytic bacterium *S. pasteurii*. Indeed, an
164 increase in pH as indicated by a colour change from orange to pink was visible as early as 1
165 h after inoculation of the plate with *S. pasteurii*, and the pH of the entire plate was alkaline by
166 24 h (Fig. 2). Similarly, the closely related ureolytic isolate CG7_3 caused a rapid increase in

167 pH, although the rate of pH change was slightly slower than seen in *S. pasteurii* (Fig. 2). The
168 same behaviour was observed for isolate EM1 (Fig. S2).

169 We next investigated the patterns of calcium carbonate precipitation on the same agar plates
170 and found that crystal formation correlated well with pH changes within the media. In non-
171 ureolytic strains, crystals were visible only on the surface of the colony, corresponding to the
172 observed localised pH change (Fig. 3A). In contrast, with ureolytic strains crystal
173 precipitation reflected the global pH change and occurred throughout the media (Fig. 3B).
174 The precipitation of calcium carbonate crystals throughout the media was likely due to a
175 change in the saturation kinetics in the media, resulting from the rapid increase in pH caused
176 by the urease-mediated release of ammonia from urea. Indeed, when urea was omitted for
177 isolate CG7_3, only the localised pH changes associated with non-ureolytic isolates was
178 seen (Fig. S3). In addition, crystals were only visible on the surface of the colony when urea
179 was omitted (Fig. S4), indicating that there are mechanistic differences in calcite precipitation
180 under ureolytic and non-ureolytic conditions.

181 Interestingly, two isolates that had tested positive for ureolysis in the test broth, CG6_1 and
182 CG4_2, did not produce the characteristic rapid rise in pH and associated crystal
183 precipitation when grown on solid media (Fig. 2 and S2). A possible explanation for this
184 discrepancy might be that in these isolates, urease activity is inducible in response to a cue
185 that was present in test broth, but not in the solid media. The main difference between the
186 two media was the content of nitrogen, which was very low in urease test broth (0.01 % (w/v)
187 yeast extract, 2 % (w/v) urea), but high in the solid media (0.2 % (w/v) yeast extract, 0.5 %
188 (w/v) peptone, 1 % (w/v) Lab-Lemco powder, 2 % (w/v) urea). Nitrogen metabolism and
189 urease production are tightly controlled in bacteria (Mobley and Hausinger, 1989). One
190 mechanism of regulation of urease is by repression of activity in the presence of ammonia-
191 or nitrogen-rich compounds and derepression of synthesis when nitrogen levels are low
192 (Mobley and Hausinger, 1989). We therefore tested to see whether nitrogen levels in the
193 media were having an effect on urease activity in these strains. Isolate CG6_1 was grown in

194 the presence of urea in media with either low (0.02 % yeast extract, 0.0125 % peptone, 2 %
195 urea) or high (0.2 % yeast extract, 0.125 % peptone, 2 % urea) nitrogen content, and urease
196 activity was quantified (Fig. 4A). Urease activity in CG6_1 was high when grown in low
197 nitrogen conditions, whilst significantly lower levels were detected in high nitrogen
198 conditions. This suggests that urease is only active in CG6_1 when the nitrogen supply is
199 limited. This is clearly a distinct type of behaviour from that seen in CG7_3 and *S. pasteurii*,
200 which both utilise urea rapidly regardless of the nitrogen composition of the media (Fig. 2).
201 However, while the overall urease activity of CG7_3 appeared similar to that of *S. pasteurii*
202 on solid media (Fig. 2), this isolate can grow well in the absence of urea (Fig. S3 and S4),
203 while *S. pasteurii* cannot. This suggests that CG7_3 may also be able to control the
204 expression of its urease genes, with urea acting directly as an inducer of urease activity. We
205 therefore tested the activity of whole cells grown in low and high nitrogen conditions as
206 before, but also compared cells grown in the presence and absence of urea (Fig. 4B). When
207 CG7_3 was grown in the absence of urea, it displayed medium urease activity under low
208 nitrogen conditions, which was further repressed by high nitrogen conditions. However,
209 when cells were grown in the presence of urea, urease activity was high regardless of
210 nitrogen conditions. Therefore, while urease activity in CG7_3 did show a partial response to
211 nitrogen limitation, this was overcome by incubation with urea, which clearly acted as the
212 main inducer and may be the preferred nitrogen source for this bacterium under the chosen
213 growth conditions. Taken together, our results indicate that there is a continuum of ureolytic
214 activity in environmental bacteria and that this, as seen above (Fig. 2-3), will have an impact
215 on crystal formation and biomineralization by different isolates.

216

217 **Effect of ureolysis on crystal formation**

218 Having established that crystal formation on solid media is very different between ureolytic
219 and non-ureolytic strains and that there are notable variations in ureolytic activity between
220 environmental isolates, we wanted to understand how ureolysis influences crystal formation

221 in more detail. To investigate this, we studied the kinetics of precipitation in our set of
222 isolates. Growing isolates in liquid culture with calcium over several days allowed us to
223 monitor the rates and total amounts of precipitate formed and correlate this to bacterial
224 growth and global pH changes. Growth of ureolytic isolates caused rapid alkalinisation of the
225 media, reaching pH 9 within two days, the first time point assayed. This resulted in complete
226 precipitation of the available calcium in the media on the same time-scale, with no further
227 change observed in two weeks of incubation (Fig. 5A and Fig. S5, *S. pasteurii*). Growth of
228 non-ureolytic bacteria caused a more gradual increase in pH, approaching pH 9 only in the
229 second week of incubation (Fig. 5B and Fig. S5). Precipitation of calcium in the media was
230 also more gradual, although both ureolytic and non-ureolytic isolates attained the maximum
231 theoretical levels of precipitation by the end of the first week. Strikingly, we observed
232 noticeable differences in cell numbers over the experimental period. Viable cell counts
233 decreased dramatically in ureolytic isolates and were undetectable within two days (Fig. 5A),
234 likely due to high ammonia concentrations in the media of these isolates resulting from the
235 cleavage of urea. Alternatively, these cells may have been encased by calcium carbonate,
236 preventing their further growth and division. In contrast, for non-ureolytic isolates cell
237 numbers gradually increased, before declining again over prolonged incubation (Fig. 5B).
238 These differences in viability over time between ureolytic and non-ureolytic bacteria may
239 have implications for application and should especially be considered in cases where the
240 continued presence of viable cells will be required for multiple cycles of precipitation.

241 Considering that the total amount of precipitate was similar in ureolytic and non-ureolytic
242 isolates, we next investigated whether the differences in the speed of precipitation had any
243 effects on the resulting crystals. As an initial observation, the precipitate recovered from
244 ureolytic strains was a much finer powder than that recovered from non-ureolytic strains.
245 EDX analyses of the different precipitates confirmed that all crystals tested were composed
246 of calcium carbonate (Fig. S6). However, further investigation using SEM revealed that the
247 crystal morphology differed between ureolytic and non-ureolytic strains (Fig. 5). When

248 precipitation was rapid, such as in ureolytic strains CG7_3 (Fig.5) and *S. pasteurii* (Fig. S5
249 and Fig S7), inorganic, homogenous crystals were produced. Non-ureolytic strains such as
250 MM1_1 that precipitated calcium carbonate more slowly produced crystals containing
251 significant proportions of bacterial cells and appeared more "organic" in nature (Fig. 5B).
252 Similarly, under these conditions CG4_2 and CG6_1 displayed the gradual increases in pH
253 (Fig. S5) and more organic precipitate characteristic of non-ureolytic strains (Fig. S7).
254 Considering that the assay conditions used for this experiment were high nitrogen, it can be
255 expected that urease activity was repressed under these conditions and resulted in strains
256 behaving like non-ureolytic strains. This differing appearance of precipitates in ureolytic
257 versus non-ureolytic conditions was consistently observed across all isolates tested in this
258 assay (Fig. S5 and Fig. S7). These results show that the differences in ureolytic activity
259 across our environmental isolates not only affected the kinetics of biomineralization, but also
260 had a clear impact on the crystal morphologies in the resulting precipitate.

261 **Profound effects of urease activity on precipitation of calcium carbonate**

262 To exclude that the observed differences in calcium carbonate precipitation were simply due
263 to strain-to-strain variation among our isolates, we exploited the fact that CG7_3 was
264 capable of switching between ureolytic and non-ureolytic states depending on the availability
265 of urea (Fig. 2 and Fig. S3). This allowed us to directly investigate the impact of ureolysis on
266 biomineralization in a single strain. When CG7_3 was grown in the absence of urea, there
267 was a gradual rise in pH and calcium carbonate precipitation as seen in non-ureolytic strains
268 (Fig. 6A). In contrast, in broths supplemented with urea we observed the rapid rise in pH and
269 associated calcium carbonate precipitation characteristic of the ureolytic strains studied
270 above (Fig. 6B). Viable cell counts also dropped dramatically in CG7_3 utilising urea (Fig.
271 6B), whereas in the absence of urea CG7_3 cell numbers remained relatively stable over the
272 first 10 days and declined by 13 days, likely due to prolonged nutrient depletion. SEM
273 analysis of the precipitates over the time-course of the study confirmed our previous
274 observations (Fig. 5) that urease activity was correlated with the rapid precipitation of

homogenous, inorganic crystals (Fig. 6B). When assessed over time, we noticed that the initial precipitate consisted of the spherical calcium carbonate, typical of the polymorph vaterite, followed by the eventual conversion into the rhombohedral morphology associated with calcite, the more stable polymorph (Fig. 6B and Fig. S8-S9). In comparison, in the absence of urea CG7_3 precipitated calcium carbonate more gradually, and these precipitates were very organic in appearance (Fig. 6A and Fig. S8-S9). Moreover, these 'organic' crystals were often much larger than the inorganic spheres produced in the presence of urea, likely due to aggregation via interspersed bacterial cells. As these experiments were all performed on the same bacterial isolate, our observations are a direct reflection of the effects of urease activity on calcite precipitation. Although both pathways produced similar quantities of precipitate, there were major differences in precipitate morphologies, number of viable bacteria and pH of the bulk phase. To our knowledge, this is the first systematic study into the fundamental differences in biomineralization between different environmental bacteria. Both ureolytic and non-ureolytic bacteria are currently being developed for a range of industrial applications (DeJong *et al.*, 2010). The findings reported here may therefore offer a key step towards a rational design approach to choosing which mechanism of biomineralization is better suited to specific industrial applications.

Industrial relevance of different calcite precipitation strategies

To test if the differences in biomineralization mechanism translate to an applied setting, we next assessed the performance of ureolytic and non-ureolytic strains in self-healing concrete applications, using cement mortars as our test system. We produced spores for each strain, which were then encapsulated in light-weight aggregate before casting them in mortars, together with yeast extract and calcium nitrate, as well as urea in the case of ureolytic strains, to provide nutrients for bacterial growth and sufficient calcium for biomineralization. Mortars were cured and then cracked under three-point bending to obtain a target crack width of 500 μM. The self-healing process was subsequently monitored over 8 weeks.

Autogenous healing, which occurs to some degree due to cement hydration, was seen in control mortars that lacked any bacterial spores (Fig. 7 and Fig. 8). This healing was mostly observed along the top edge of the crack and rarely extended down the sides of the mortar prism. Mortars containing either ureolytic or non-ureolytic bacteria also displayed crack healing, and this generally extended across the top as well as down the sides of the crack (Fig. 7 and Fig. 8). However, healing in mortars containing ureolytic bacteria was less regular than seen with non-ureolytic strains, with the sides of cracks not consistently sealing (Fig. 8).

The key aim of bacteria-induced self-healing of concrete is to re-establish water tightness of the structure to prevent water ingress and subsequent corrosion of steel reinforcement. While visual inspection allowed an initial assessment of the healing process, we next sought to test water tightness of our mortars using water flow tests following eight weeks of healing. Recovery of water tightness in mortars containing only the standard cement mix, with no nutrients or additional calcium showed variable recovery of water tightness, generally close to 40 % (Fig. 9, ‘Reference’). Control mortars containing yeast extract and calcium nitrate, but without bacterial spores, showed much higher recovery (averaging 87-95 %). This recovery is likely because of a combination of autogenous healing and possible presence of environmental bacteria, which may be able to utilise the yeast extract and thus contribute to precipitation. As the mortars were not made or kept in a sterile fashion to more closely reflect industrial application, contamination with such environmental bacteria must be considered likely. The mortars containing non-ureolytic bacteria showed a strikingly consistent recovery in water tightness, leading to near complete resistance to water flow, with all specimens healing to over 90 % and many reaching close to 100% (Fig. 9). Interestingly, while mortars containing ureolytic bacteria also showed good restoration of water tightness, there was more variation in the degree of healing obtained. EM1 performed as well as the non-ureolytic strains, but CG7_3 showed lower overall recovery values (mean 87 %) that were similar to the controls lacking encapsulated bacteria. This discrepancy in results may reflect the

329 variability in ureolytic activity in these strains. Given the clear dependence on growth
330 conditions in some strains described above, it is difficult to predict the degree of ureolytic
331 ability displayed in cement mortars. An alternative explanation may be that the rapid
332 precipitation and small crystal size observed in ureolytic isolates does not reliably lead to
333 retention of the precipitate within the crack and may thus not perform as reliably in self-
334 healing as the larger aggregates with organic components of the non-ureolytic strains. It will
335 be interesting to investigate the details of material performance following healing with both
336 types of bacteria to fully understand the implications of the different mechanisms of
337 precipitation.

338

339 **CONCLUDING REMARKS**

340 The environment represents a large reservoir of potential in terms of exploiting bacteria for
341 commercial use of MICP. There have been numerous studies on MICP for varying
342 applications, however, most of these have been restricted to the use of a single or small
343 number of species and were very application specific. This limits our understanding of
344 precipitation capabilities of environmental bacteria more generally. In order to establish a
345 stronger knowledge base to facilitate new and specialised technical applications we
346 surveyed the ability of environmental bacteria to precipitate calcite. We found that the
347 majority of isolates were capable of biomineralization, in line with previous results (Boquet *et*
348 *al.*, 1973). This is most likely due to their ability, through metabolic processes, to create a
349 microenvironment around the cell that aids in the precipitation process. The electronegative
350 nature of their cell surface facilitates crystal deposition on the surface (Schultze-Lam *et al.*,
351 1996), making precipitation more favourable. Our detailed characterisation of
352 biomineralization by our set of isolates, however, revealed fundamental differences in the
353 way in which different bacteria precipitate calcium carbonate.

354 Ureolytic bacteria rapidly precipitate calcium carbonate, having led to ureolysis becoming
355 one of the main pathways used in MICP applications to date. However, in our study, only 16
356 % of isolates were able to cleave urea, and even amongst these there was a marked
357 diversity in ureolytic activity. Differences in how isolates regulate urease activity were seen,
358 with some responding to low nitrogen levels whilst others responded to urea as a primary
359 inducer. This was in striking contrast to the constitutive high urease activity of *S. pasteuri*,
360 one of the most frequently utilised MICP-capable bacteria to date (Stocks-Fischer *et al.*,
361 1999; Tobler *et al.*, 2011; Zhu *et al.*, 2016). The performance of ureolytic bacteria will
362 therefore depend on the precise conditions encountered in their environment, and this
363 should be carefully considered when choosing the bacterial species for a given application.
364 The importance of this point is further emphasised by our finding that ureolysis affected
365 crystal formation both in terms of kinetics and in the morphology of the precipitate.

366 The majority of our isolates precipitated calcium carbonate without possessing ureolytic
367 activity. In contrast to initial expectations that this mechanism may lead to the formation of
368 low amounts of precipitate, we found that all of our isolates were capable of precipitating the
369 total amount of calcium supplied in the growth media, although this process took more time
370 with non-ureolytic strains. Importantly, we showed that the precipitate formed by the non-
371 ureolytic bacteria consisted of larger, mixed organic/inorganic crystals. This was in good
372 agreement with our initial observation that precipitation in these bacteria on solid media only
373 occurred on top of the colony and therefore likely involved the physical presence of cells.
374 The mixed nature of the precipitate means that for the same amount of calcium being used,
375 a larger volume of precipitate can be formed. This could present a major advantage in
376 industrial application where often only a limited amount of calcium is available to fill a
377 relatively large space, such as in self-healing concrete.

378 When we tested the performance of our isolates in self-healing of cracked cement mortars,
379 we found that, indeed, non-ureolytic bacteria caused a more consistent recovery of water
380 tightness and more complete healing. The ureolytic bacteria tested showed less consistency

381 in performance, although one strain gave similar results to the non-ureolytic isolates. It is
382 difficult to ascertain whether these inconsistencies in behaviour are due to differences in
383 ureolytic activity in the applied setting or are a consequence of the purely inorganic
384 precipitate formed by ureolytic strains. It seems plausible that the supply of yeast extract as
385 part of the cement mix will lead to a low-nitrogen environment conducive to urease gene
386 expression, and the presence of urea should ensure activity in those strains that are urea-
387 responsive. While further experimentation is needed to determine the precise conditions
388 encountered by the bacteria within hardened cement mortars as well as the material
389 properties of the precipitate formed, in applications where nutritional supply is hard to
390 control, the use of non-ureolytic bacteria may give more robust and reliable performance.

391 Self-healing concrete of course only represents one of many potential applications of MICP
392 and each application will have its own challenges. For example, in spray-on applications
393 such as restoration of existing structures and historic buildings, the rapid precipitation of
394 large amounts of precipitate through ureolysis may be advantageous. In contrast, during soil
395 stabilisation where bacteria and their substrates are pumped into the ground, rapid rates of
396 ureolysis could result in premature precipitation and lead to blockages at the injection site as
397 has been reported (Cheng and Cord-Ruwisch, 2014). In this case, it would be more
398 beneficial to use microbes that are non-ureolytic, or that switch to ureolysis at a later time
399 point, as seen in our isolates that responded to low environmental nitrogen.

400 In summary, most bacteria have the ability to precipitate calcium carbonate given the right
401 conditions, and the most suitable bacteria to use will be application dependent. While most
402 previous studies have focussed on one or two isolates, we here show for the first time the
403 plethora of MICP activities and capabilities the environment has to offer as a 'talent pool' that
404 can offer bespoke solutions to many different applications. MICP-based technologies may
405 offer solutions to problems caused by a rising global population and may even be used to
406 mitigate global warming. The increasing demand for infrastructure, as well as the need to
407 engineer land on which to build it, results in an increase in CO_2 emissions and release of

408 harmful chemicals into the environment (DeJong *et al.*, 2010). MICP can reduce this
409 environmental burden by producing buildings that are more durable, prolonging the life of
410 existing buildings, and improving soil properties without the use of toxic and hazardous
411 chemical additives. Moreover, technologies that actively remove CO_2 from the environment
412 and sequestrate it in harmless or even useful minerals such as calcite will be critical in
413 meeting zero emission goals in the future.

414

415 **EXPERIMENTAL PROCEDURES**

416 **Bacterial isolates and growth**

417 Sample collection was from six locations across the United Kingdom including limestone
418 caves and immature calcareous soils (Mendip Hills, England), soil, rock and limestone caves
419 (Bath, England), soil and rock scrapings (Monmouthshire, Wales) and soil and scrapings
420 from marine rock in two locations in Cornwall (Mount's Bay and Falmouth). Samples were
421 stored at 4°C until use. Of each sample, 0.5 g was re-suspended in 1 ml sterile saline
422 solution (0.85% (w/v) NaCl) and heated to 80°C for 20 minutes to enrich for spore-formers.
423 Selection for alkali-tolerant bacteria was carried out by plating 100 µl of this suspension onto
424 0.25× B4 medium (1 g l^{-1} yeast extract, 12 g l^{-1} Trizma base, 1.25 g l^{-1} glucose, 2.5 g l^{-1}
425 calcium acetate ($Ca(OAc)_2$), 15 g l^{-1} agar) adjusted with NaOH to pH 9. Glucose and
426 $Ca(OAc)_2$ were filter-sterilised and added after autoclaving. Individual colonies with unique
427 colony morphology were re-streaked onto 0.25× B4 medium buffered with 75 mM CHES, 75
428 mM CAPS, adjusted with NaOH to pH 10. Strains capable of growth at pH 10 and with
429 visible crystals on the colony or in the surrounding agar were selected for further
430 characterisation. Single colonies were inoculated in lysogeny broth (LB; 10 g l^{-1} tryptone, 5 g
431 l^{-1} yeast extract, 10 g l^{-1} NaCl) and grown overnight, before storage at -80 °C in a 25% (w/v)
432 glycerol solution. Isolates were subsequently maintained on LB agar.
433 *Sporosarcina pasteurii* DSM33 was included as a reference organism and maintained on LB

434 agar supplemented with 20 g l^{-1} urea (filter-sterilized, added after autoclaving). All bacterial
435 cultures were grown at 30 °C, and liquid cultures were agitated at 150 rpm. Growth of liquid
436 cultures was monitored spectrophotometrically by optical density at 600 nm wavelength
437 (OD_{600}) in cuvettes of 1 cm light path length. Representative isolates showing the best
438 characteristics were deposited into the DSMZ collection (Deutsche Sammlung von
439 Mikroorganismen und Zellkulturen GmbH, Germany) as follows*: DSM XX (RC1_1), DSM
440 XX (PD1_1), DSM XX (EM1), DSM XX (CG7_3), DSM XX (CG7_2), DSM XX (CG6_1), DSM
441 XX (CG4_2), and DSM XX (MM1_1).

442 **Note to reviewers: The DSM numbers have not yet been issued but will be available by the*
443 *time the manuscript has been through the review process.*

444

445 **Identification of isolates and phylogenetic analysis**

446 The 16S rDNA gene fragment was amplified using the 27F (5'-
447 AGAGTTTGATCMTGGCTCAG-3') and 1492R (5'-TACCTTGTTACGACTT- 3') primers
448 (Lane, 1991). Amplification was performed in a total volume of 25 µl containing 12.5 µl of 2x
449 OneTaq Mastermix (New England Biolabs, NEB), 9.9 µl of nuclease-free H_2O, 2.4 % (v/v)
450 DMSO, 0.2 µM of each primer and 1 µl of an overnight culture as template. Reaction
451 conditions were as follows: initial denaturation at 94 °C for 5 min followed by 30 cycles
452 consisting of denaturation at 94°C for 30 sec, annealing at 45° C for 30 sec, and extension
453 at 68 °C for 2 min. Final extension was at 68°C for 5 min. For enzymatic clean-up, 2 µl of
454 EXO-SAP (100 U shrimp alkaline phosphatase (Thermo Scientific), 100 U Exonuclease I
455 (Thermo Scientific), and 895 µl nuclease-free H_2O) was added to every 5 µl of PCR product
456 and the reaction was incubated at 37°C for 15 min before enzyme inactivation at 80°C for 15
457 min. Sequencing of PCR products was carried out using the chain termination method
458 (Eurofins Genomics, Germany). In the case of strains where direct sequencing of the PCR
459 product was unsuccessful, 16S rDNA fragments were first cloned into the Topo® vector

460 according to manufacturer's instructions (TOPO TA Cloning® Kit, Invitrogen). Sequencing of
461 the resulting plasmids was performed using the M13 forward primer (5'-
462 CCCAGTCACGACGTTGTAAAACG-3'). Bioedit (Hall, 1999) was used to assemble
463 sequences obtained from forward and reverse sequencing reactions. Sequences were
464 compared against the non-redundant GenBank nucleotide collection using BLASTN
465 (http://www.ncbi.nlm.nih.gov). For phylogenetic analyses, the 16S rDNA sequences of
466 nearest relatives for each strain according to BLASTN analysis, as well as of
467 *Sporosarcina pasteurii* DSM 33 were obtained from GenBank, and evolutionary analyses
468 were carried out in MEGA 7.0 (Kumar *et al.*, 2016). Sequences were aligned using
469 MUSCLE, and conserved blocks were selected from these multiple alignments using
470 GBlocks (Castresana, 2000). Phylogenetic trees were constructed using the maximum
471 likelihood (ML) method based on the Tamura-Nei model (Tamura and Nei, 1993). Bootstrap
472 values were inferred from 1000 replicates and partitions reproduced in less than 50 %
473 bootstrap replicates were collapsed.

474

475 **Analysis of calcium carbonate precipitation**

476 Spatial distribution of calcite precipitation and pH changes was assessed by spotting 20 µl of
477 an overnight culture (OD_{600} adjusted to 1) onto nutrient agar (Oxoid, 23 g l^{-1}) supplemented
478 with phenol red (0.025 g l^{-1}) and $Ca(OAc)_2$ (2.5 g l^{-1} or 10 g l^{-1}), with or without urea (20 g l^{-1}).
479 Physical appearance of plates and crystals were recorded photographically at 1 hr, 3 hr, 5
480 hr, 24 hr, and 48 hr.

481 Rate of mineral precipitation over time was determined by inoculating (1:1000) 150 ml LB
482 broth supplemented with 10 g l^{-1} $Ca(OAc)_2$ from overnight cultures and monitoring viable cell
483 numbers, pH, and insoluble calcium precipitated over time. Viable cells were determined as
484 colony-forming units (CFU) by the plate count method. pH was recorded from aliquots of the
485 culture using a pH electrode (Jenway 924 030, Cole-Parmer, Staffordshire UK) coupled to a

486 pH meter (Jenway 3510 pH Meter). Insoluble precipitate was recovered by centrifugation
487 (975 × *g*, 2 minutes at room temperature (RT)) and washed three times in 50 ml distilled
488 water to remove planktonic cells and culture medium before oven drying at 50 °C for 48
489 hours. Morphology of dried precipitates was examined at accelerating voltages ranging from
490 10 to 20 kV by scanning electron microscopy (SEM; JSM 6480LV, JEOL, Welwyn, UK)
491 equipped with an energy dispersive x-ray (EDX) analyser for elemental analysis.
492 Representative samples were prepared by spreading dried precipitate on double-sided
493 carbon tape placed on aluminium stubs. For EDX, samples were placed under vacuum
494 overnight before analysis. For imaging, samples were gold-coated by sputtering for 3 min at
495 RT. Samples imaged with field emission electron microscopy (FE-SEM; JSM-6301F cold
496 field emission SEM, JEOL) were prepared in a similar manner as for SEM but coated in
497 Chromium to a thickness of 20 nM and examined at 5 kV.

498

499 **Urease activity**

500 Qualitative urease activity of bacterial isolates was determined using urease test broth (0.1 g
501 l^{-1} yeast extract, 20 g l^{-1} urea, 0.01 g l^{-1} phenol red, 0.67 mM KH_2PO_4, 0.67 mM Na_2HPO_4 (pH
502 6.8±0.2). Test broth (2 ml) was inoculated with 100 µl of an overnight culture grown in LB
503 and incubated at 30 °C for up to 5 days. A urease-positive reaction was characterised by a
504 change in colour from yellow/orange to pink.

505 For quantitative urease measurements in whole cells, cultures were grown at 30 °C with
506 agitation (150 rpm). Overnight cultures (20 µl, LB broth) were used to inoculate 25 ml (1:500)
507 low nitrogen (0.2 g l^{-1} yeast extract, 0.125 g l^{-1} peptone, 2.5 g l^{-1} NaCl) and standard media
508 (2 g l^{-1} yeast extract, 1.25 g l^{-1} peptone, 2.5 g l^{-1} NaCl) broths. Where pre-induction by urea
509 was required, broths were supplemented with urea (20 g l^{-1}). Cultures were grown (for 24 hr)
510 and cells were harvested from 1 ml of culture by centrifugation (8000 *x g*, 2 min). Cells were
511 resuspended in 1 volume 0.1 M potassium phosphate buffer (pH 8.0), and OD_{600} was

512 recorded. Depending on the urease activities of individual strains, dilutions of cells were
513 made to ensure the activity was within the linear range of the assay. These dilutions were
514 recorded and accounted for during OD normalisation. Urease activity was determined
515 according to the phenol-hypochlorite method (Natarajan, 1995) and adapted from (Achal *et*
516 *al.*, 2009) for whole cells. The reaction mix volumes were multiplied by the number of time-
517 points in the assay to allow one larger volume mix to be prepared. Per time point, individual
518 reactions contained 75 µl cell suspension, 300 µl 0.1 M potassium phosphate buffer (pH 8.0)
519 and 750 µl 0.1 M urea solution. The mixture was incubated at 30°C and 1 ml aliquots were
520 removed at 0, 30, 60, 90 and 120 min. At each time point, the reaction was stopped by
521 adding 300 µl phenol nitroprusside and 300 µl alkaline hypochlorite. Final colour was
522 developed at 37 °C for 25 min and absorbance was measured at 625 nm. Ammonium
523 chloride (25-2500 µM) solutions were used to produce a standard curve (Fig. S1). One unit
524 of activity was defined as the release of 1 µM of ammonia per minute, per OD (U OD^{-1} ml^{-1}).

525

526 **Endospore production**

527 Endospores of bacterial strains were prepared by inoculating 150 ml LB broth (1:1000) from
528 an overnight culture grown at 30°C with shaking (150 rpm). This culture was again grown
529 overnight and then cells were harvested by centrifugation (3200 × *g*, 10 min at RT) and
530 resuspended in 750 ml Difco sporulation medium (DSM; 8 g l^{-1} nutrient broth (Oxoid), 13.41
531 mM KCl, 0.49 mM $MgSO_4$, adjusted to pH 7.6 with NaOH. Prior to use 1mM $Ca(NO_3)_2$, 0.01
532 mM $MnCl_2$, and 1µM $FeSO_4$ were added from a filter-sterilised stock solution (Sonenshein *et*
533 *al.*, 1974). Cultures were grown with agitation (150 rpm) at 30 °C for at least 48 hours before
534 sporulation was assessed using phase contrast microscopy. When the majority of cells
535 contained phase-bright endospores, cells were pelleted by centrifugation (3200 × *g*, 10 min
536 at RT) and washed thrice in 10 mM Tris-HCl (pH 9) followed by 30 min treatment with
537 chlorohexidine digluconate (0.3 mg ml^{-1}) to kill vegetative cells. Washing was repeated as

before and spore pellets were snap-frozen in liquid nitrogen and freeze-dried under vacuum overnight.

Preparation of mortar samples

Mortar prisms (65 mm × 40 mm × 40 mm) were comprised of two layers. The first contained (per 3 prisms): 253.3 g sand conforming to BS EN 196-1, 92 g Portland limestone cement (CEM II A-L 32.5R), 46 g water, 1 g yeast extract, 4.55 g calcium nitrate, 3.54 g aerated concrete granules. Mortars containing ureolytic bacteria also contained urea (3.68 g per 3 prisms). Spores (2.1 x 10^{10} cfu) were resuspended in 1 ml dH_2O and imbibed into the aerated concrete granules before drying and sealing with polyvinyl acetate (PVA, 30% (w/w)). After approximately 3 hours, the second, top layer was cast. The second layer contained standard cement mortar (Per 3 prisms: 276g standard sand, 92 g cement, 46 g water). Reference specimens were cast in two layers but only contained standard cement mortar. Specimens remained at room temperature for 24-48 hours before demoulding and subsequent curing for 28 days submersed in tap water. After curing, specimens were oven dried at 50 °C for 24 hours. The top third of the prism was wrapped with carbon fibre reinforced polymer strips to enable generation of a crack of controlled width. A notch (1.5 mm deep) was sawn at mid-span to serve as a crack initiation point. Specimens were cracked by three-point bending using a 30 kN Instron static testing frame. A crack mouth opening displacement (CMOD) gauge was used to measurement crack width. Load was applied to maintain a crack growth of 25 μm per minute, and loading was stopped when the crack width was predicted to be 500 μm wide after load removal. A marker pen was used to indicate specific crack sections to enable monitoring of the crack at the same site. Following cracking, prisms were placed in tanks, open to the atmosphere and filled with tap water to 1 cm below the top of the mortars, and were incubated at room temperature for two months. Visualisation of crack healing was monitored using a Leica M205C light microscope, and images were taken of freshly cracked mortars and after 1, 4, and 8 weeks of healing.

Water permeability tests

Water flow rate before cracking, after cracking, and after 8 weeks of healing was determined to monitor effects of cracking and healing on water permeability in mortars as described previously (Lee and Ryou, 2016). The instrument used was based on RILEM test method II.4 (RILEM, 1987). The bottom of a 10 ml measuring cylinder (0.2 ml graduation) was removed and a 40 mm PVC pipe with 15 mm depth was fixed to the bottom. This was sealed onto the mortar with glue. This cylinder was filled with water and the time it took to drop from initial height h_1 to a final height h_2 was recorded. The total height was either 78.5 mm or, in the case of samples with low permeability, the height to which the water level had dropped after 30 min. The permeability coefficient was calculated according to Equation 3 (Lee and Ryou, 2016).

$$k = \frac{aL}{At} ln\left[\frac{h_1}{h_2}\right], \quad (3)$$

where k = water permeability coefficient (cm/s); a = cross-sectional area of the cylinder (1.77 cm^2); L = thickness of specimen (4 cm); A = cross-sectional area of the specimen which equals the cross-sectional area of acrylic plate (10.18 cm^2); t = time (s); h_1 = initial water head (12.4 cm); h_2 = final water head (cm). The percentage of crack healing was calculated as follows:

$$\text{Healing percentage } (\%) = \frac{(k_0 - k_t)}{k_0} \text{ x } 100 \quad (4)$$

where k_0 = initial water permeability after cracking, k_t = water permeability at healing time t.

ACKNOWLEDGEMENTS

The authors would like to acknowledge the Engineering and Physical Sciences Research Council (EPSRC; EP/PO2081X/1) and industrial collaborators/partners for funding the

589 Resilient Materials for Life (RM4L) project. TDH was supported by a University of Bath
590 Research Studentship Award. We thank technical staff in the Department of Architecture and
591 Civil Engineering and the Department of Biology and Biochemistry for key support. We
592 further thank Dr Philip Fletcher and Diane Lednitzky of the Material and Chemical
593 Characterisation Facility (MC^2) at University of Bath (https://doi.org/10.15125/mx6j-3r54) for
594 their assistance with microscopy.

595

596 **REFERENCES**

597 Achal, V., Mukherjee, A., Basu, P.C., and Reddy, M.S. (2009) Lactose mother liquor as an
598 alternative nutrient source for microbial concrete production by *Sporosarcina pasteurii*.
599 *J Ind Microbiol Biotechnol* **36**: 433–438.

600 Achal, V., Pan, X., and Zhang, D. (2011) Remediation of copper-contaminated soil by
601 *Kocuria flava* CR1 , based on microbially induced calcite precipitation. *Ecol Eng* **37**:
602 1601–1605.

603 Alazhari, M., Sharma, T., Heath, A., Cooper, R., and Paine, K. (2018) Application of
604 expanded perlite encapsulated bacteria and growth media for self-healing concrete.
605 *Constr Build Mater* **160**: 610–619.

606 Altermann, W., Kazmierczak, J., Oren, A., and Wright, D.T. (2006) Cyanobacterial
607 calcification and its rock- building potential during 3.5 billion years of Earth history.
608 *Geobiology* **4**: 147–166.

609 Bang, S.S., Lippert, J.J., Yerra, U., Mulukutla, S., and Ramakrishnan, V. (2010) Microbial
610 calcite , a bio-based smart nanomaterial in concrete remediation. *Int J Smart Nano*
611 *Mater* **1**: 28–39.

612 Boquet, E., Boronat, A., and Ramos-Cormenzana, A. (1973) Production of Calcite (Calcium
613 Carbonate) Crystals by Soil Bacteria is a General Phenomenon. *Nature* **246**: 527–529.

614 Castresana, J. (2000) Selection of Conserved Blocks from Multiple Alignments for Their Use
615 in Phylogenetic Analysis. *Mol Biol Evol* **17**: 540–552.

616 Ceci, A., Pinzari, F., Riccardi, C., Maggi, O., Pierro, L., Papini, M.P., et al. (2018) Metabolic
617 synergies in the biotransformation of organic and metallic toxic compounds by a
618 saprotrophic soil fungus. *Environ Biotechnol* **102**: 1019–1033.

619 Cheng, L. and Cord-Ruwisch, R. (2014) Upscaling Effects of Soil Improvement by
620 Microbially Induced Calcite Precipitation by Surface Percolation. *Geomicrobiol J* **31**:
621 396–406.

622 DeJong, J.T., Mortensen, B.M., Martinez, B.C., and Nelson, D.C. (2010) Bio-mediated soil
623 improvement. *Ecol Eng* **36**: 197–210.

624 Hall, T. (1999) Bioedit: a user-friendly biological sequence alignment editor and analysis
625 program for Windows 95/98/NT. *Nucleic Acids Symp Ser* **41**: 95–98.

626 Hammes, F. and Verstraete, W. (2002) Key roles of pH and calcium metabolism in microbial

627 carbonate precipitation. *Rev Environ Sci Biotechnol* **1**: 3–7.

628 Huntzinger, D.N. and Eatmon, T.D. (2009) A life-cycle assessment of Portland cement
629 manufacturing : comparing the traditional process with alternative technologies. *J Clean*
630 *Prod* **17**: 668–675.

631 Jonkers, H.M., Thijssen, A., Muyzer, G., Copuroglu, O., and Schlangen, E. (2010)
632 Application of bacteria as self-healing agent for the development of sustainable
633 concrete. *Ecol Eng* **36**: 230–235.

634 Kumar, S., Stecher, G., and Tamura, K. (2016) MEGA7 : Molecular Evolutionary Genetics
635 Analysis Version 7 . 0 for Bigger Datasets Brief communication. *Mol Biol Evol* **33**:
636 1870–1874.

637 Lane, D. (1991) 16S/23S rRNA sequencing. In, Stackebrandt,E. and Goodfellow,M. (eds),
638 *Nucleic acid techniques in bacterial systematics*. John Wiley and Sons, pp. 115–175.

639 Lee, Y.S. and Ryou, J.S. (2016) Crack healing performance of PVA-coated granules made
640 of cement, CSA, and Na2CO3 in the cement matrix. *Materials (Basel)* **9**: 555–575.

641 Mitchell, A.C., Dideriksen, K., Spangler, L.H., Cunningham, A.B., and Gerlach, R. (2010)
642 Microbially Enhanced Carbon Capture and Storage by Mineral-Trapping and Solubility-
643 Trapping. *Environ Sci Technol* **44**: 5270–5276.

644 Mobley, H.L.T. and Hausinger, R.P. (1989) Microbial Ureases : Significance , Regulation ,
645 and Molecular Characterization. *Microbiol Rev* **53**: 85–108.

646 Natarajan, K.R. (1995) Kinetic Study of the Enzyme Urease from Dolichos biflorus. *J Chem*
647 *Educ* **72**: 556–557.

648 Power, I.M., Wilson, S.A., Small, D.P., Dipple, G.M., Wan, W., and Southam, G. (2011)
649 Microbially Mediated Mineral Carbonation : Roles of Phototrophy and Heterotrophy.
650 *Environ Sci Technol* **45**: 9061–9068.

651 RILEM (1987) Measurement of Water Absorption Under Low Pressure. RILEM Test Method
652 No. 11.4.

653 Schultze-Lam, S., Fortin, D., Davis, B.S., and Beveridge, T.J. (1996) Mineralization of
654 bacterial surfaces. *Chem Geol* **132**: 171–181.

655 Sharma, T.K., Alazhari, M., Heath, A., Paine, K., and Cooper, R.M. (2017) Alkaliphilic
656 *Bacillus* species show potential application in concrete crack repair by virtue of rapid
657 spore production and germination then extracellular calcite formation. *J Appl Microbiol*
658 **122**: 1233–1244.

659 Sonenshein, A.L., Cami, B., Brevet, J., and Cote, R. (1974) Isolation and Characterization of
660 Rifampin-Resistant and Streptolydigin-Resistant Mutants of *Bacillus subtilis* with Altered
661 Sporulation Properties. *J Bacteriol* **120**: 253–265.

662 Souto-Martinez, A., Arehart, J.H., and Srubar III, W. V (2018) Energy & Buildings Cradle-to-
663 gate CO_2 emissions vs . *in situ* CO_2 sequestration of structural concrete elements.
664 *Energy Build* **167**: 301–311.

665 Stocks-Fischer, S., Galinat, J.K., and Bang, S.S. (1999) Microbiological precipitation of
666 $CaCO_3$. *Soil Biol Biochem* **31**: 1563–1571.

667 Tamura, K. and Nei, M. (1993) Estimation of the Number of Nucleotide Substitutions in the
668 Control Region of Mitochondrial DNA in Humans and. *Mol Biol Evol* **10**: 512–526.

669 Tobler, D.J., Cuthbert, M.O., Greswell, R.B., Riley, M.S., Renshaw, J.C., Handley-Sidhu, S.,
670 and Phoenix, V.R. (2011) Comparison of rates of ureolysis between *Sporosarcina*

671 *pasteurii* and an indigenous groundwater community under conditions required to
672 precipitate large volumes of calcite. *Geochim Cosmochim Acta* **75**: 3290–3301.

673 Wang, J., De Belie, N., and Verstraete, W. (2012) Diatomaceous earth as a protective
674 vehicle for bacteria applied for self-healing concrete. *Biotechnol Methods* **39**: 567–577.

675 Wang, J., Jonkers, H.M., Boon, N., and De Belie, N. (2017) *Bacillus sphaericus* LMG 22257
676 is physiologically suitable for self-healing concrete. *Appl Microbiol Biotechnol* **101**:
677 5101–5114.

678 Wilmeth, D.T., Johnson, H.A., Stamps, B.W., Berelson, W.M., Stevenson, B.S., Nunn, H.S.,
679 et al. (2018) Environmental and Biological Influences on Carbonate Precipitation Within
680 Hot Spring Microbial Mats in Little Hot Creek, CA. *Front Microbiol* **9**: 1–13.

681 Zhao, Q., Li, L., Asce, M., Li, C., Li, M., Amini, F., et al. (2014) Factors Affecting
682 Improvement of Engineering Properties of MICP-Treated Soil Catalyzed by Bacteria
683 and Urease. *J Mater Civ Eng* **26**: 1–10.

684 Zhu, T., Dittrich, M., and Dittrich, M. (2016) Carbonate Precipitation through Microbial
685 Activities in Natural environment , and Their Potential in Biotechnology : A Review.
686 *Front Bioeng Biotechnol* **4**: 1–21.

687

688 **FIGURE LEGENDS**

689 **Figure 1. Phylogenetic analysis of selected calcite-precipitating isolates and their**
690 **closest relatives.** Yellow boxes, non-ureolytic isolates; orange boxes, isolates with inducible
691 ureolytic activity; pink boxes, isolates that utilize urea as a primary nitrogen source; unfilled
692 boxes, unknown ureolytic ability. The ureolytic potential of closest relatives is not shown.
693 Accession numbers are indicated in parentheses. The percentage of trees in which
694 associated taxa clustered together is shown next to the branches (1000 bootstraps).

695 **Figure 2. Diversity in ureolytic activity across environmental isolates.** *Left*, urease test
696 broth inoculated with the strains indicated to the left. *Right*, nutrient agar plates
697 supplemented with phenol red, calcium acetate, and urea were inoculated in the centre with
698 suspensions of the same strains. Pink shading indicates the pH change caused by ammonia
699 release from ureolytic activity.

700 **Figure 3. Crystal formation correlates with pH changes in non-ureolytic and ureolytic**
701 **bacteria.** (A) Non-ureolytic isolate PD1_1 shows localised crystals on the bacterial colony.
702 (B) Ureolytic *S. pasteurii* demonstrates crystal precipitation throughout the media,

703 corresponding to pH changes that occur throughout the media. Arrows indicate $CaCO_3$
704 crystals.

705 **Figure 4. Regulation of urease activity by environmental nitrogen and urea.** Isolates
706 CG6_1 (A) and CG7_3 (B) cells were grown in high or low nitrogen conditions in the
707 presence (+) or absence (-) of urea. Error bars represent standard deviation from 2-3
708 biological reps with 1-2 technical reps each. Significance was tested using an unpaired t-test
709 (A) and one-way ANOVA followed by unpaired t-test (B). *, P <0.05, ***, P <0.001 and ****, P
710 <0.0001.

711 **Figure 5. Calcite precipitation kinetics and crystal morphology in ureolytic CG7_3 and**
712 **non-ureolytic MM1_1.** The ureolytic strain CG7_3 (A) and the non-ureolytic MM1_1 (B)
713 were grown in LB medium supplemented with urea (20 g l^{-1}) and $Ca(OAc)_2$ (10 g l^{-1}) and
714 precipitation of insoluble calcium carbonate (bars, g l^{-1}), pH changes (circles) and changes in
715 cell number (boxes, CFU ml^{-1}) were monitored over time (days). Maximum theoretical level
716 of precipitation is indicated (dotted line). *Right,* electron micrographs of representative
717 precipitate taken at day 9.

718 **Figure 6. Comparison of ureolytic and non-ureolytic mechanisms of calcite**
719 **precipitation in CG7_3.** The ureolytic strain CG7_3 was grown in LB medium
720 supplemented with $Ca(OAc)_2$ (10 g l^{-1}) in the absence (A) and presence (B) of urea (20 g l^{-1}).
721 Precipitation of insoluble calcium carbonate (bars, g l^{-1}), pH changes (circles) and changes
722 in cell number (boxes, CFU ml^{-1}) were monitored over time (days). Maximum theoretical
723 level of precipitation is indicated (dotted line). *Right,* electron micrographs of representative
724 precipitate taken at days 3 and 13.

725 **Figure 7. Crack closure in control mortars and mortars containing non-ureolytic**
726 **bacteria.** Cracks in mortar specimens are shown immediately post-cracking and after 8
727 weeks of healing. Cracks were marked with black pen to allow the same region to be
728 monitored over time. Two independent regions along the top of the mortar were monitored

729 per sample. Side views show the cracks down both sides of the mortar at 8 weeks. *White*
730 *arrows*, complete crack closure. *Black arrows*, incomplete crack closure.

731 **Figure 8. Crack closure in control mortars and mortars containing ureolytic bacteria.**
732 Cracks in mortar specimens are shown immediately post-cracking and after 8 weeks of
733 healing. Cracks were marked with black pen to allow the same region to be monitored over
734 time. Two independent regions along the top of the mortar were monitored per sample. Side
735 views show the cracks down both sides of the mortar at 8 weeks. *White arrows*, complete
736 crack closure. *Black arrows*, incomplete crack closure.

737 **Figure 9. Recovery of water tightness in mortars after two months of bacteria-based**
738 **self-healing**. Water flow through mortars containing ureolytic (CG7_3, EM1) or non-ureolytic
739 (MM1_1, RC1_1) bacteria was determined immediately after cracking and following 8 weeks
740 of healing. Reference mortars contained no additives; Control mortars contained yeast
741 extract and calcium nitrate, but no bacteria. Recovery of water tightness was determined as
742 a percentage relative to the freshly cracked specimen (0%: no change in water flow, 100%:
743 complete inhibition of water flow). Data is shown for four specimens per condition from two
744 separate cracking/healing experiments.

745

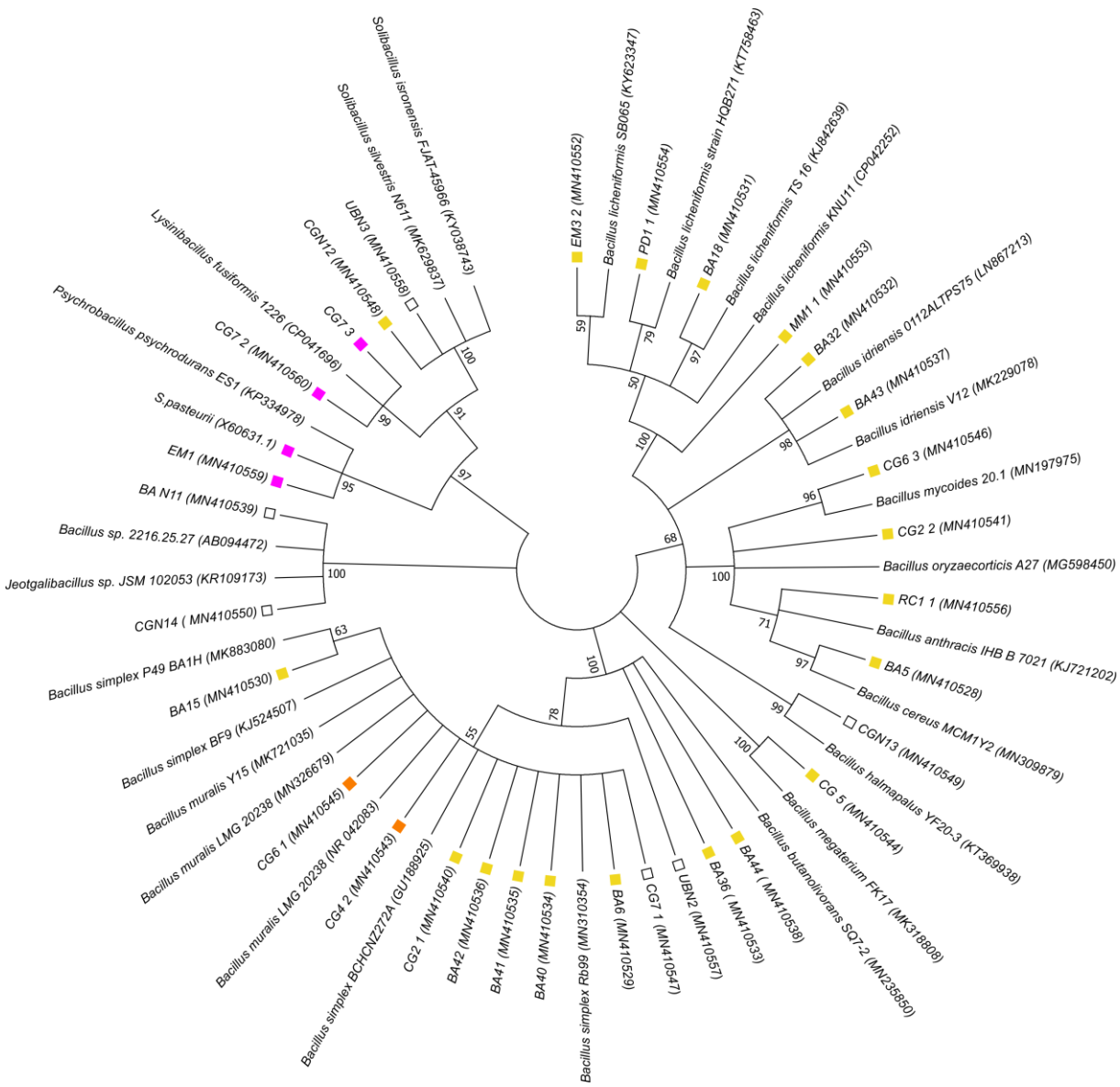

Figure 1. Phylogenetic analysis of selected calcite-precipitating isolates and their closest relatives. Yellow boxes, non-ureolytic isolates; orange boxes, isolates with inducible ureolytic activity; pink boxes, isolates that utilize urea as a primary nitrogen source; unfilled boxes, unknown ureolytic ability. The ureolytic potential of closest relatives is not shown. Accession numbers are indicated in parentheses. The percentage of trees in which associated taxa clustered together is shown next to the branches (1000 bootstraps).

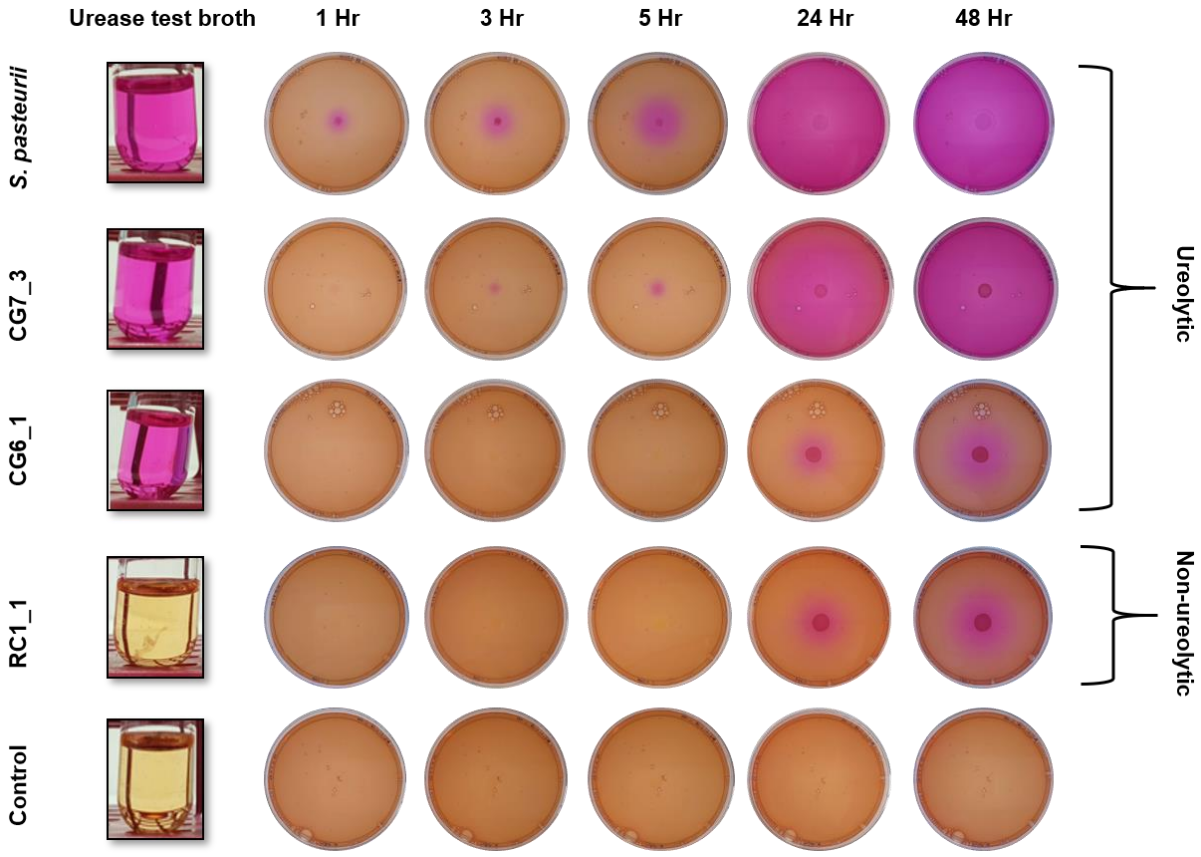

Figure 2. Diversity in ureolytic activity across environmental isolates. *Left*, urease test broth inoculated with the strains indicated to the left. *Right*, nutrient agar plates supplemented with phenol red, calcium acetate, and urea were inoculated in the centre with suspensions of the same strains. Pink shading indicates the pH change caused by ammonia release from ureolytic activity.

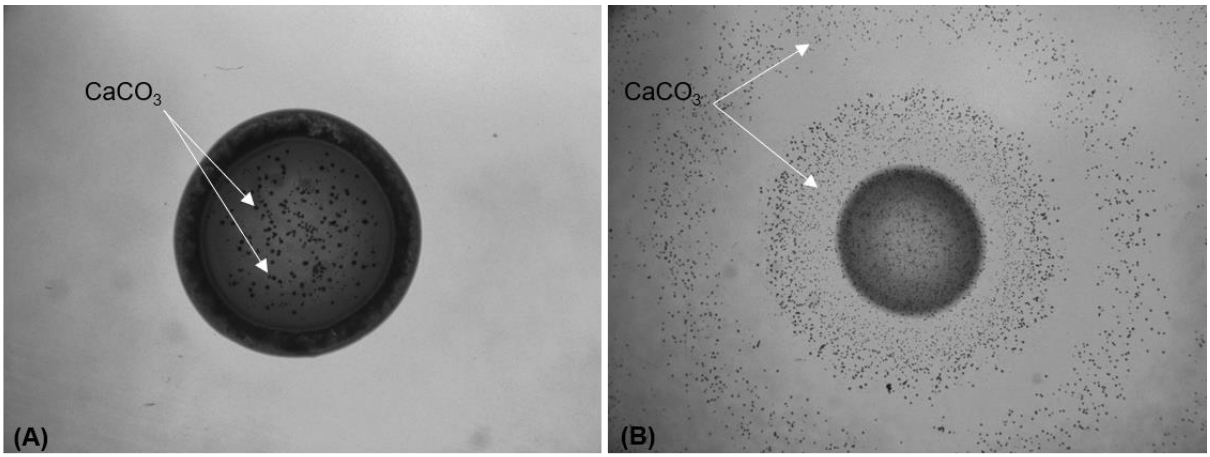

Figure 3. Crystal formation correlates with pH changes in non-ureolytic and ureolytic bacteria. (A) Non-ureolytic isolate PD1_1 shows localised crystals on the bacterial colony. (B) Ureolytic *S. pasteurii* demonstrates crystal precipitation throughout the media, corresponding to pH changes that occur throughout the media. Arrows indicate $CaCO_3$ crystals.

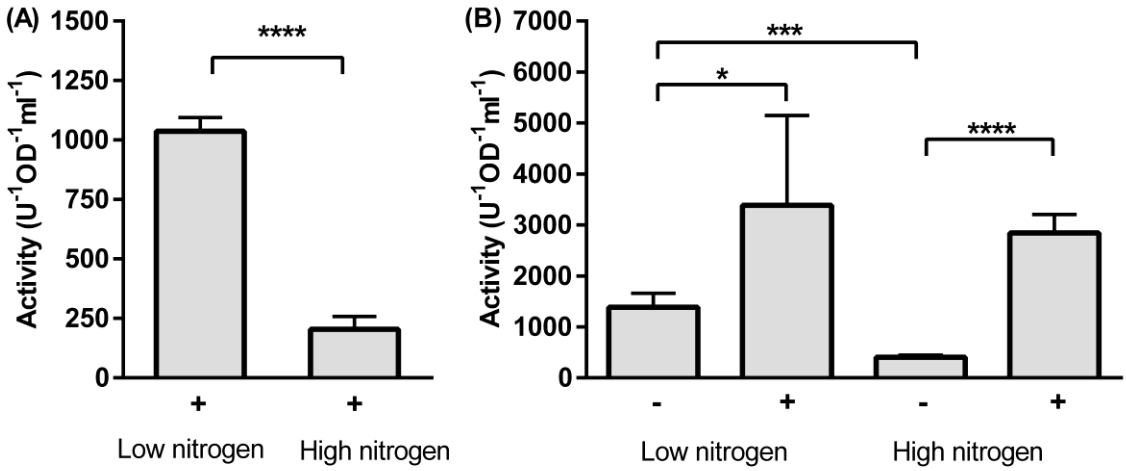

Figure 4. Regulation of urease activity by environmental nitrogen and urea. Isolates CG6_1 (A) and CG7_3 (B) cells were grown in high or low nitrogen conditions in the presence (+) or absence (-) of urea. Error bars represent standard deviation from 2-3 biological reps with 1-2 technical reps each. Significance was tested using an unpaired t-test (A) and one-way ANOVA followed by unpaired t-test (B). *, P <0.05, ***, P <0.001 and ****, P <0.0001.

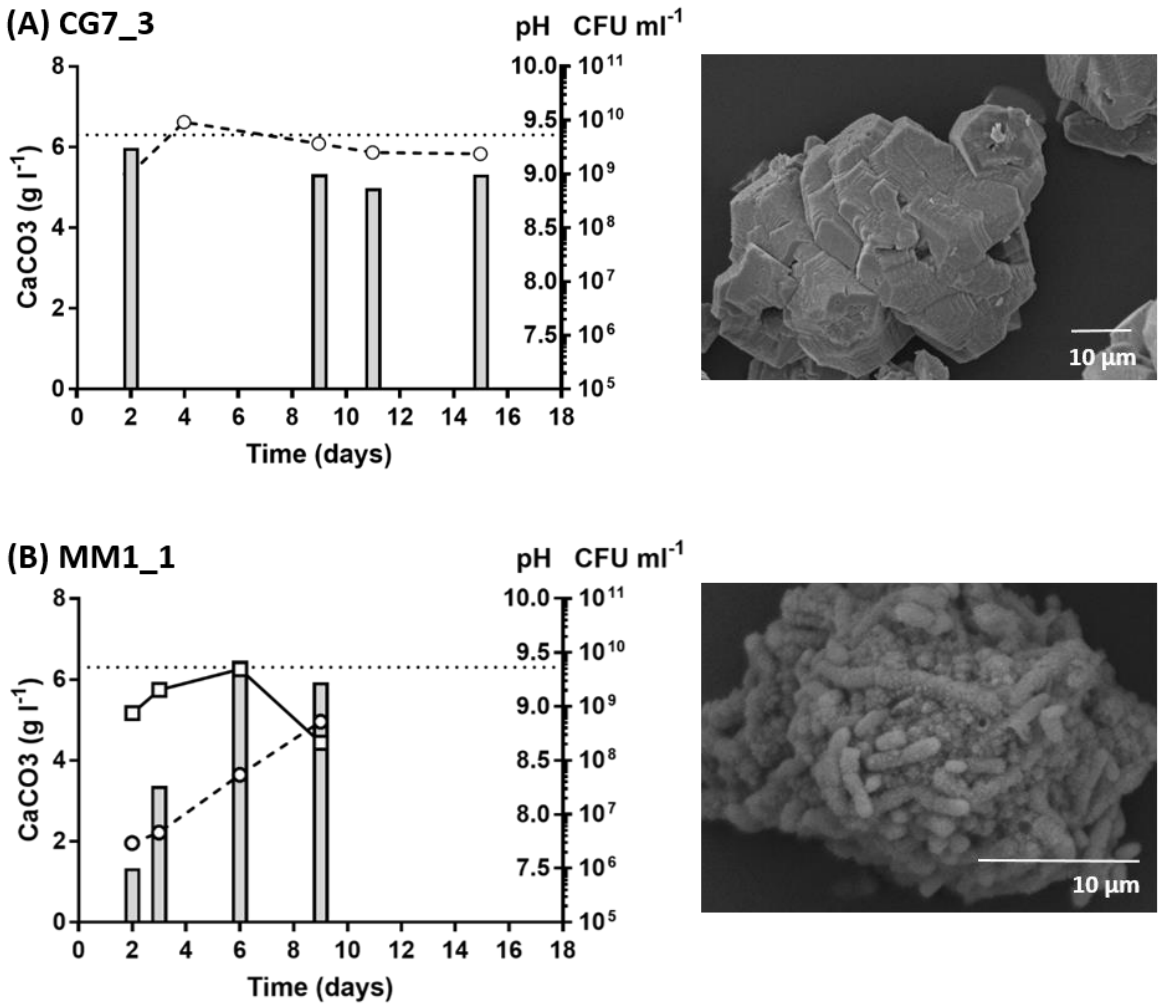

Figure 5. Calcite precipitation kinetics and crystal morphology in ureolytic CG7_3 and non-ureolytic MM1_1. The ureolytic strain CG7_3 (A) and the non-ureolytic MM1_1 (B) were grown in LB medium supplemented with urea (20 g l^{-1}) and $Ca(OAc)_2$ (10 g l^{-1}) and precipitation of insoluble calcium carbonate (bars, g l^{-1}), pH changes (circles) and changes in cell number (boxes, CFU ml^{-1}) were monitored over time (days). Maximum theoretical level of precipitation is indicated (dotted line). *Right,* electron micrographs of representative precipitate taken at day 9.

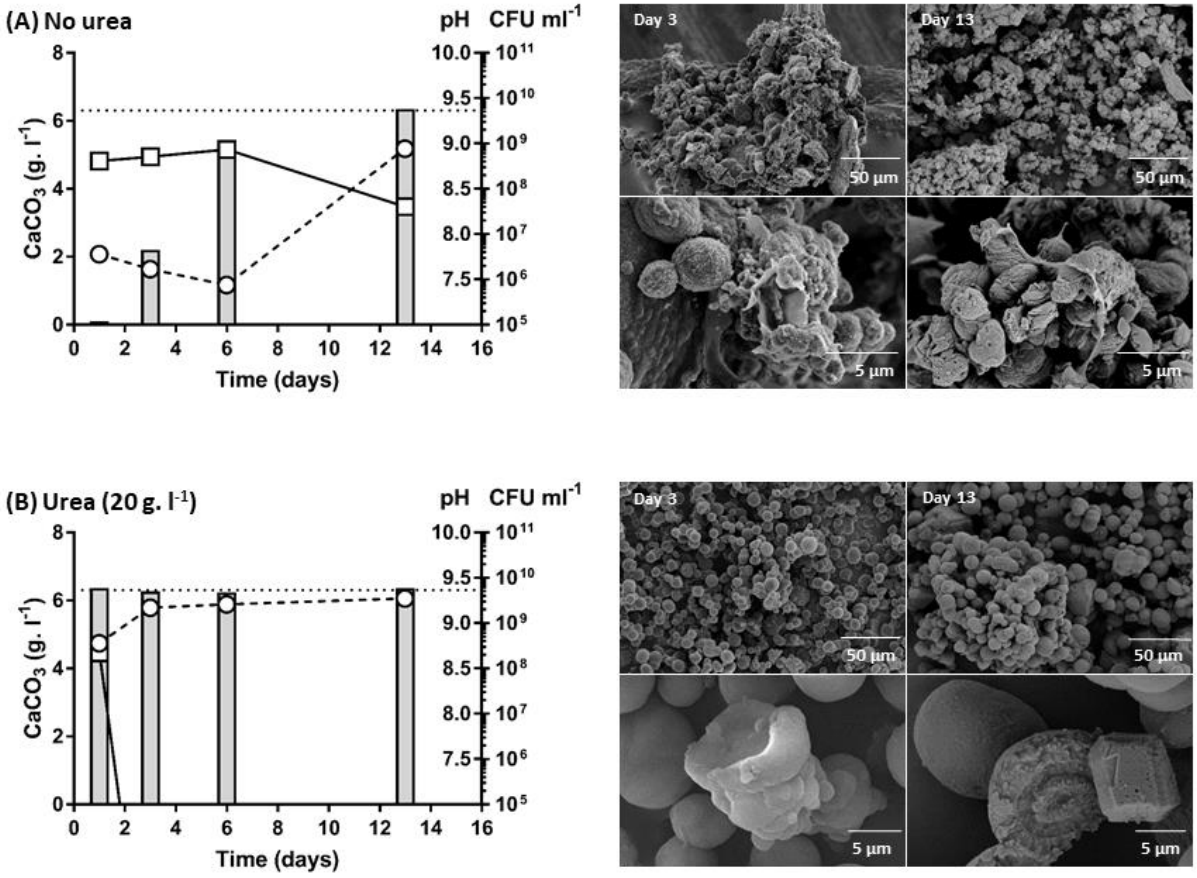

Figure 6. Comparison of ureolytic and non-ureolytic mechanisms of calcite precipitation in CG7_3. The ureolytic strain CG7_3 was grown in LB medium supplemented with $Ca(OAc)_2$ (10 g l^{-1}) in the absence (A) and presence (B) of urea (20 g l^{-1}). Precipitation of insoluble calcium carbonate (bars, g l^{-1}), pH changes (circles) and changes in cell number (boxes, CFU ml^{-1}) were monitored over time (days). Maximum theoretical level of precipitation is indicated (dotted line). *Right,* electron micrographs of representative precipitate taken at days 3 and 13.

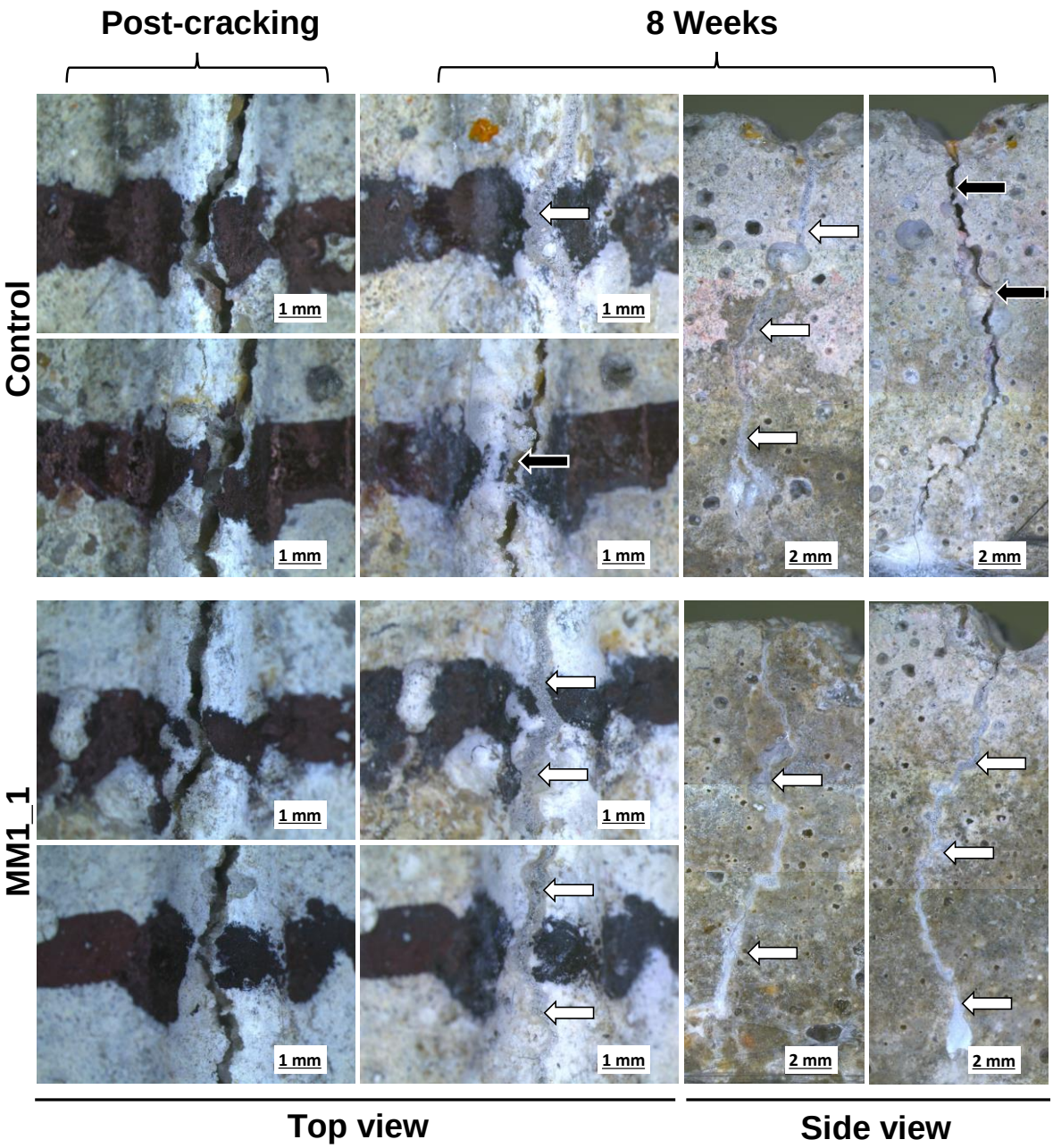

Figure 7. Crack closure in control mortars and mortars containing non-ureolytic bacteria. Cracks in mortar specimens are shown immediately post-cracking and after 8 weeks of healing. Cracks were marked with black pen to allow the same region to be monitored over time. Two independent regions along the top of the mortar were monitored per sample. Side views show the cracks down both sides of the mortar at 8 weeks. *White arrows*, complete crack closure. *Black arrows*, incomplete crack closure.

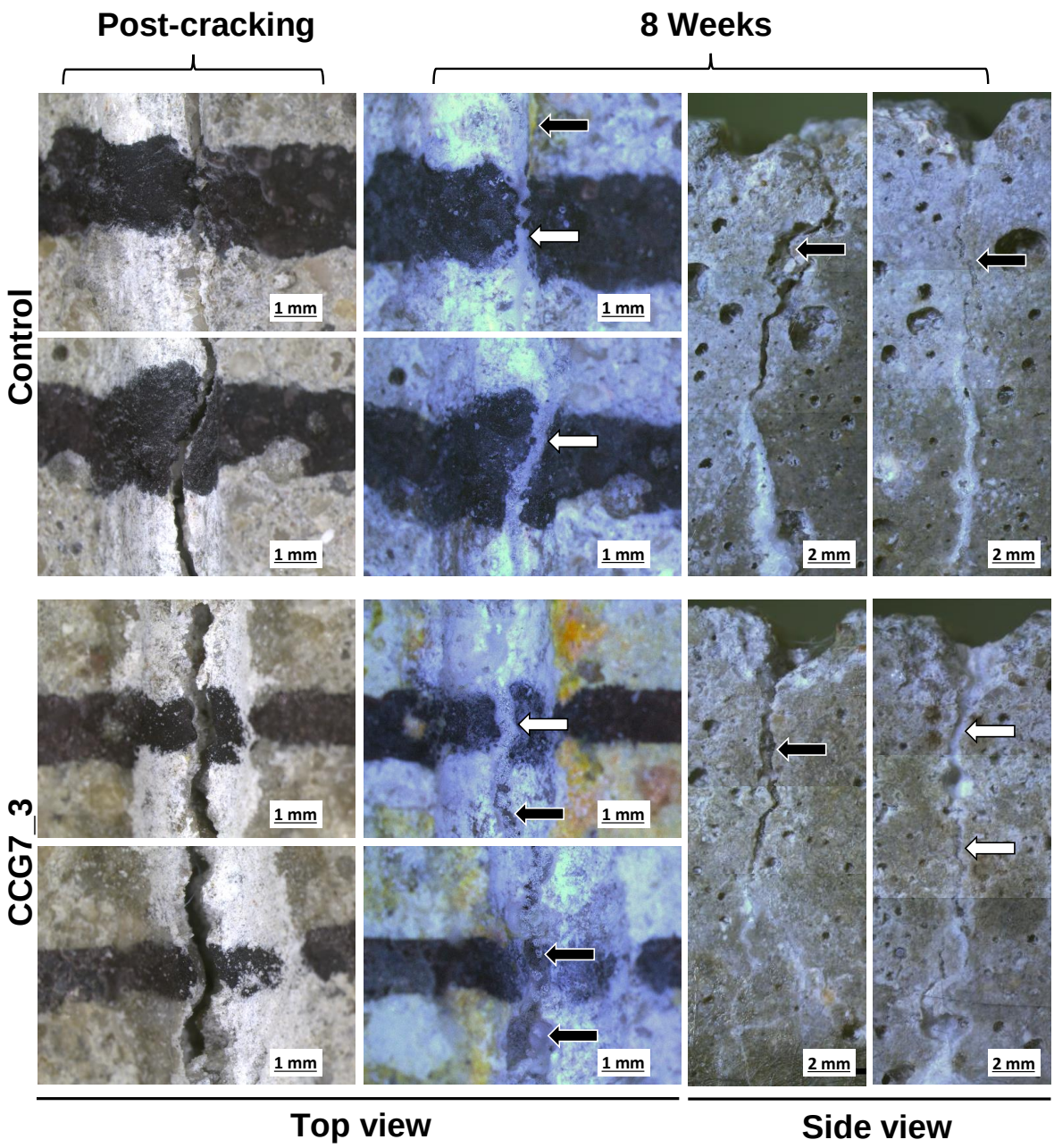

Figure 8. Crack closure in control mortars and mortars containing ureolytic bacteria. Cracks in mortar specimens are shown immediately post-cracking and after 8 weeks of healing. Cracks were marked with black pen to allow the same region to be monitored over time. Two independent regions along the top of the mortar were monitored per sample. Side views show the cracks down both sides of the mortar at 8 weeks. *White arrows*, complete crack closure. *Black arrows*, incomplete crack closure.

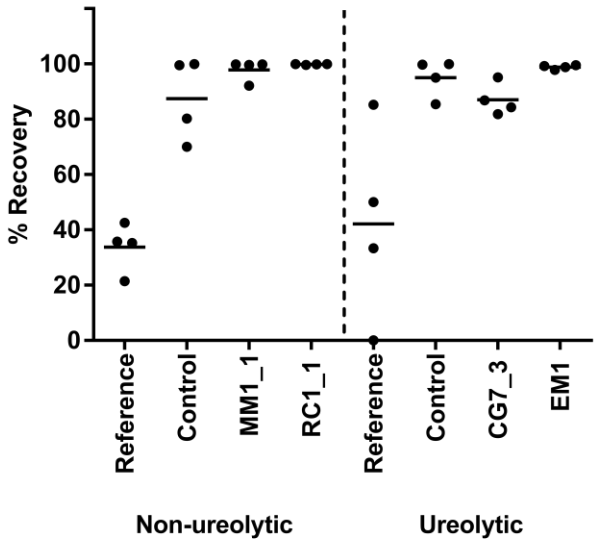

Figure 9. Recovery of water tightness in mortars after two months of bacteria-based self-healing. Water flow through mortars containing ureolytic (CG7_3, EM1) or non-ureolytic (MM1_1, RC1_1) bacteria was determined immediately after cracking and following 8 weeks of healing. Reference mortars contained no additives; Control mortars contained yeast extract and calcium nitrate, but no bacteria. Recovery of water tightness was determined as a percentage relative to the freshly cracked specimen (0%: no change in water flow, 100%: complete inhibition of water flow). Data is shown for four specimens per condition from two separate cracking/healing experiments.

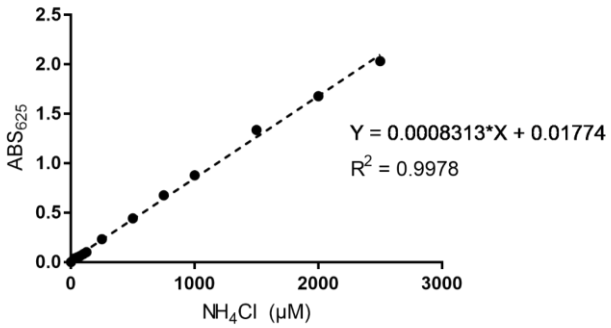

Figure S1. Ammonium chloride concentration vs absorbance standard curve. Ammonium chloride (25-2500 µM) solutions were used as standards to quantify the change in absorbance at 625 nm wavelength (A_{625}) observed using phenol-hypochlorite as described in methods. The linear fit of ammonium chloride concentration versus absorbance used to calculate unknown concentrations is shown by the equation and dashed line.

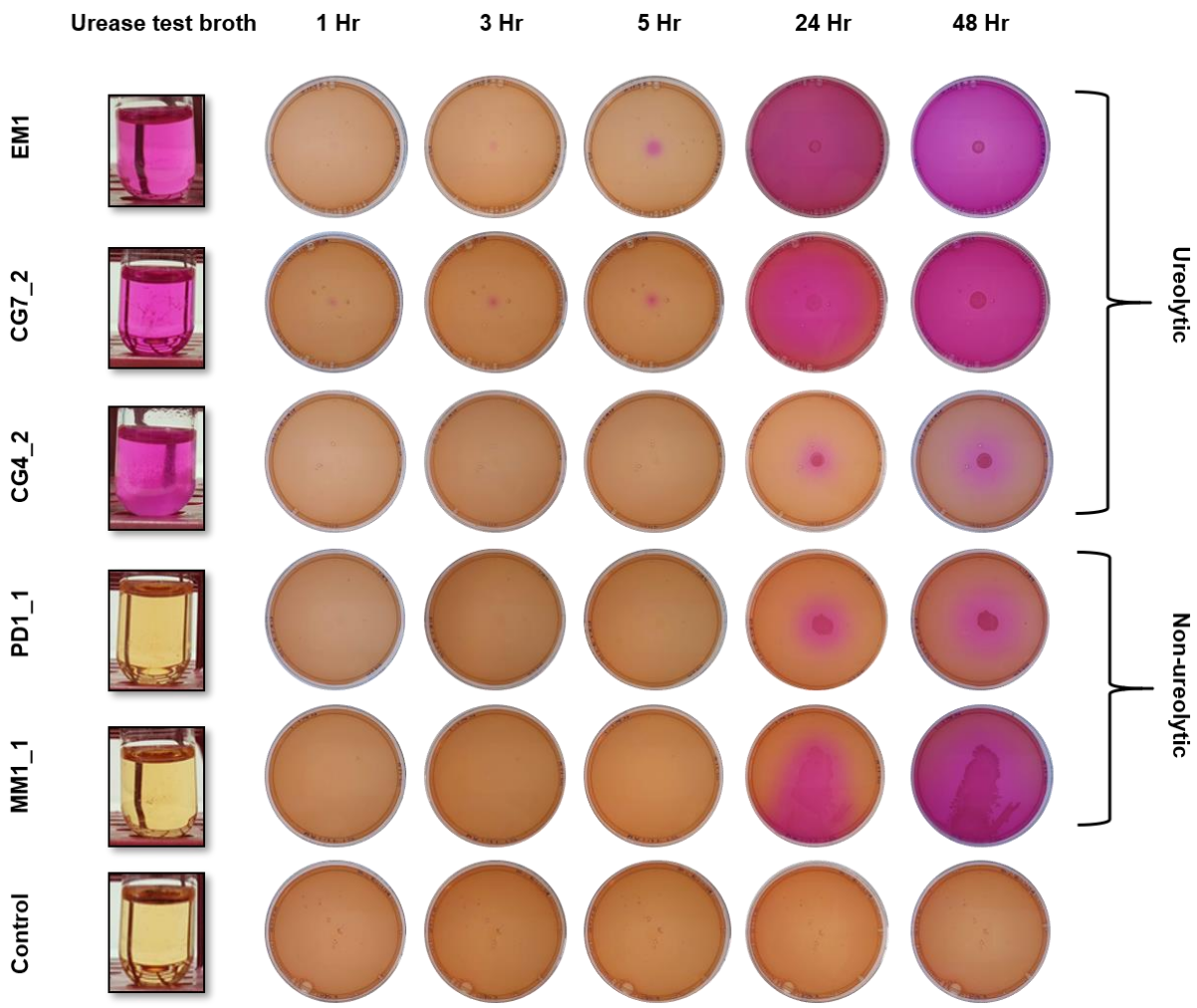

Figure S2. Diversity in ureolytic activity across environmental isolates. *Left*, urease test broth inoculated with the strains indicated to the left. *Right*, nutrient agar plates supplemented with phenol red, calcium acetate, and urea were inoculated in the centre with suspensions of the same strains. Pink shading indicates the pH change caused by ammonia release from ureolytic activity. MM1_1, although non-ureolytic, caused changes in pH likely due to a stress response to urea which resulted in swarming.

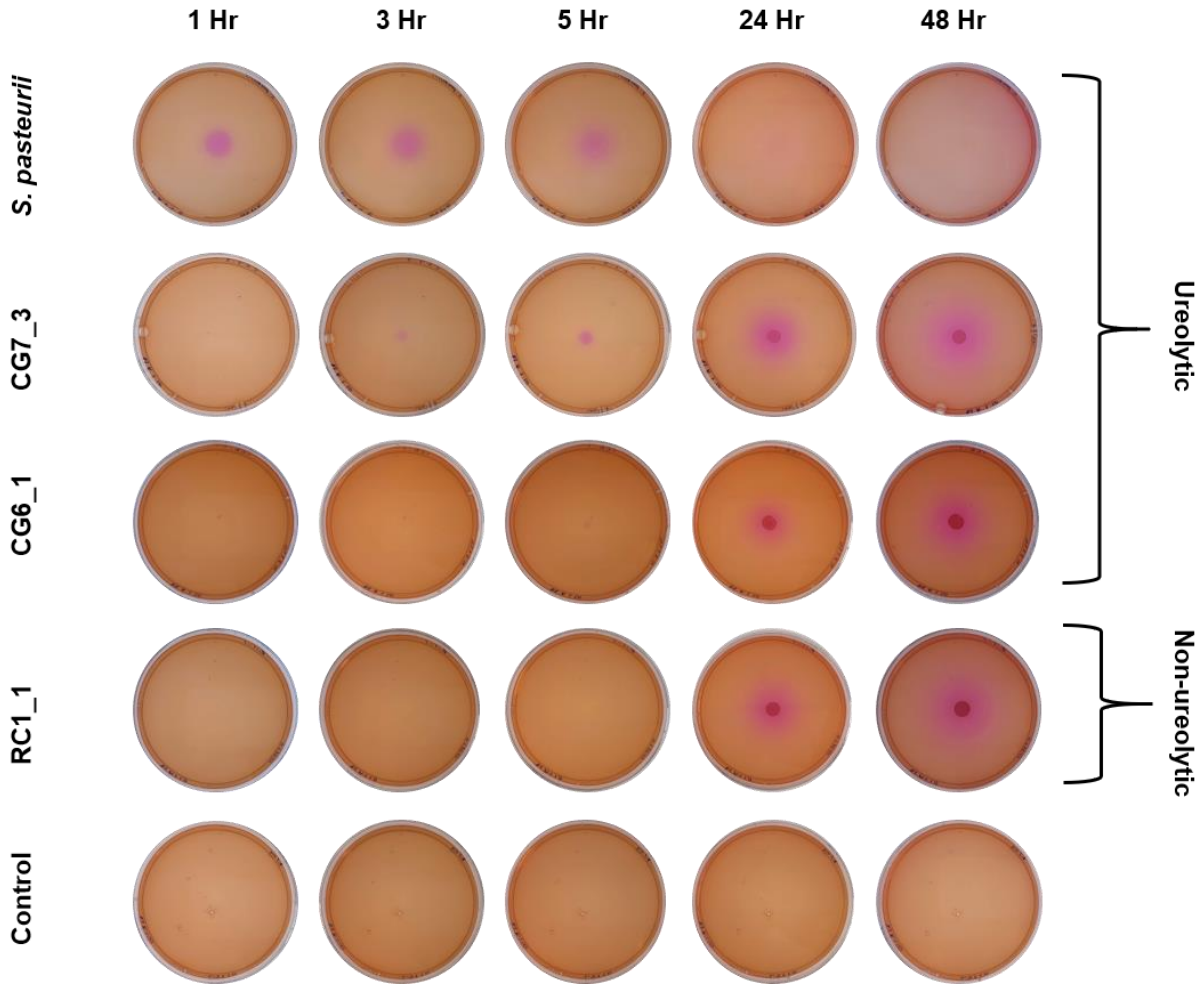

Figure S3. No pH changes are seen in ureolytic isolates when urea is excluded from the media. Nutrient agar plates supplemented with phenol red and calcium acetate were inoculated in the centre with suspensions of the same strains. Only local pH changes characteristic of normal metabolism are seen.

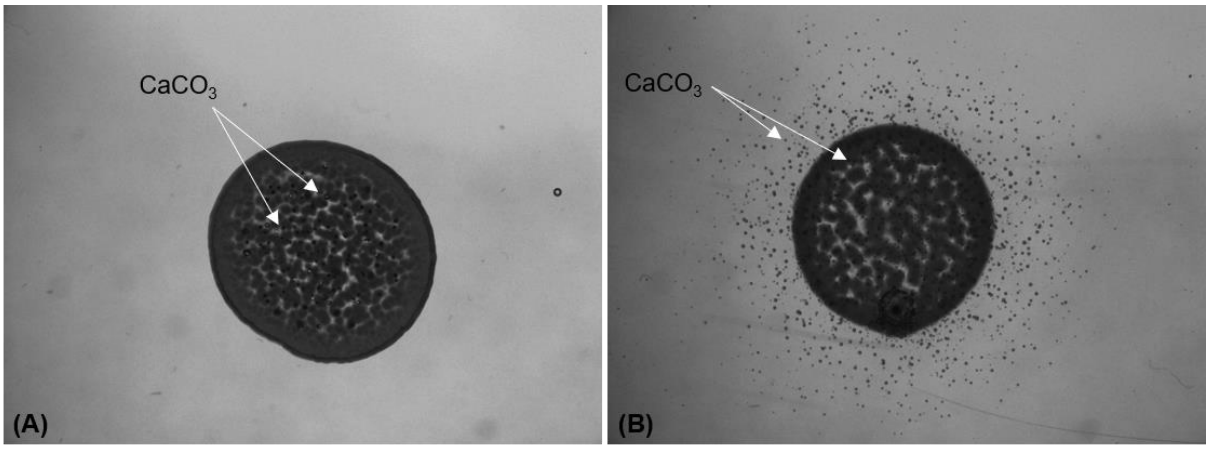

Figure S4. Comparison of crystal localisation in ureolytic strain CG7_3 without (A) and with (B) urea. Ureolytic bacteria precipitate crystals locally in the absence of urea, similar to what is seen in non-ureolytic strains. Arrows indicate $CaCO_3$ crystals.

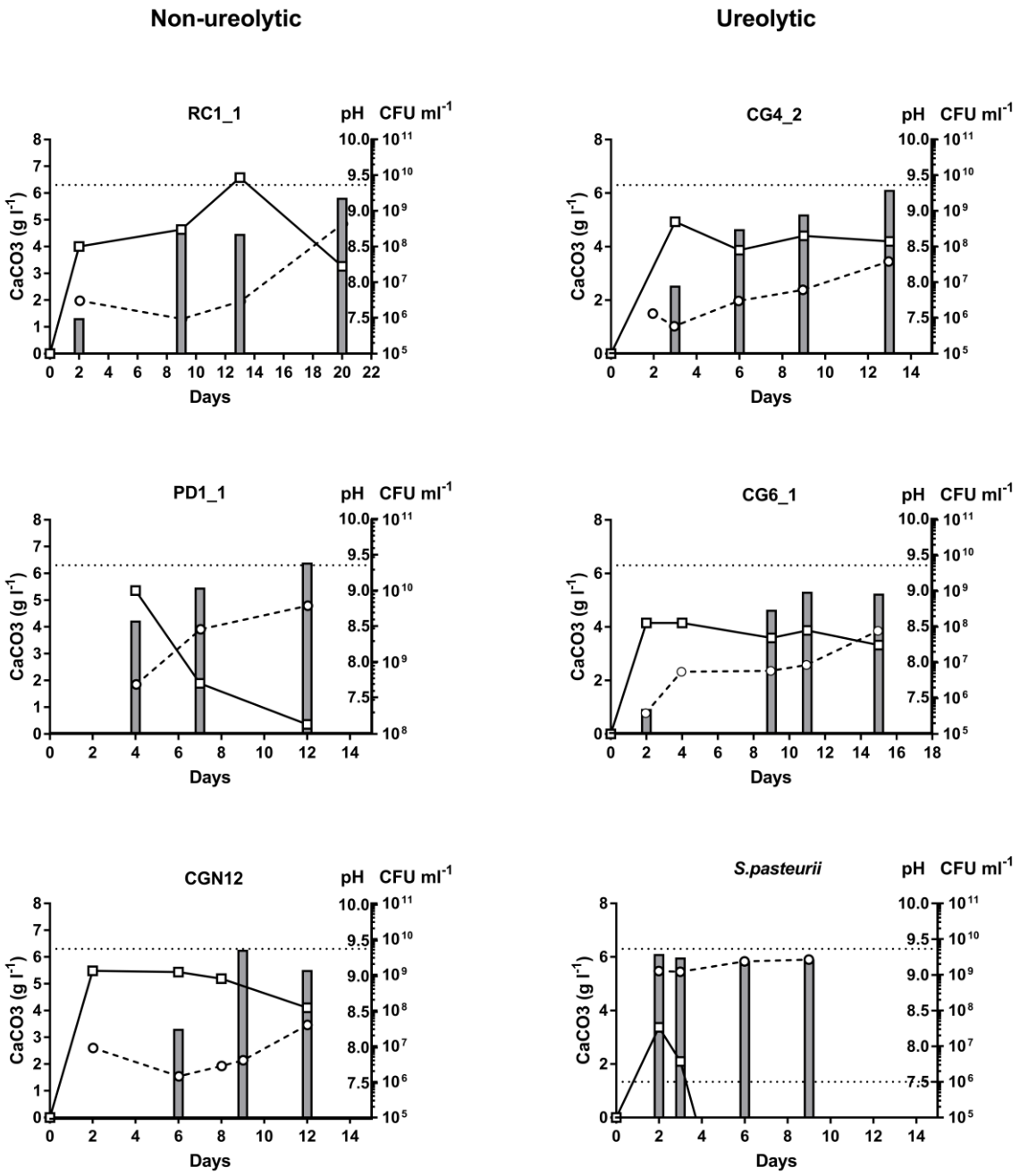

Figure S5. Calcite precipitation kinetics in ureolytic and non-ureolytic isolates. Isolates were grown in LB medium supplemented with urea (20 g l^{-1}) and CaAoc (10 g l^{-1}) and precipitation of insoluble calcium carbonate (bars, g l^{-1}), pH changes (circles) and changes in cell number (boxes, CFU ml^{-1}) were monitored over time (days).

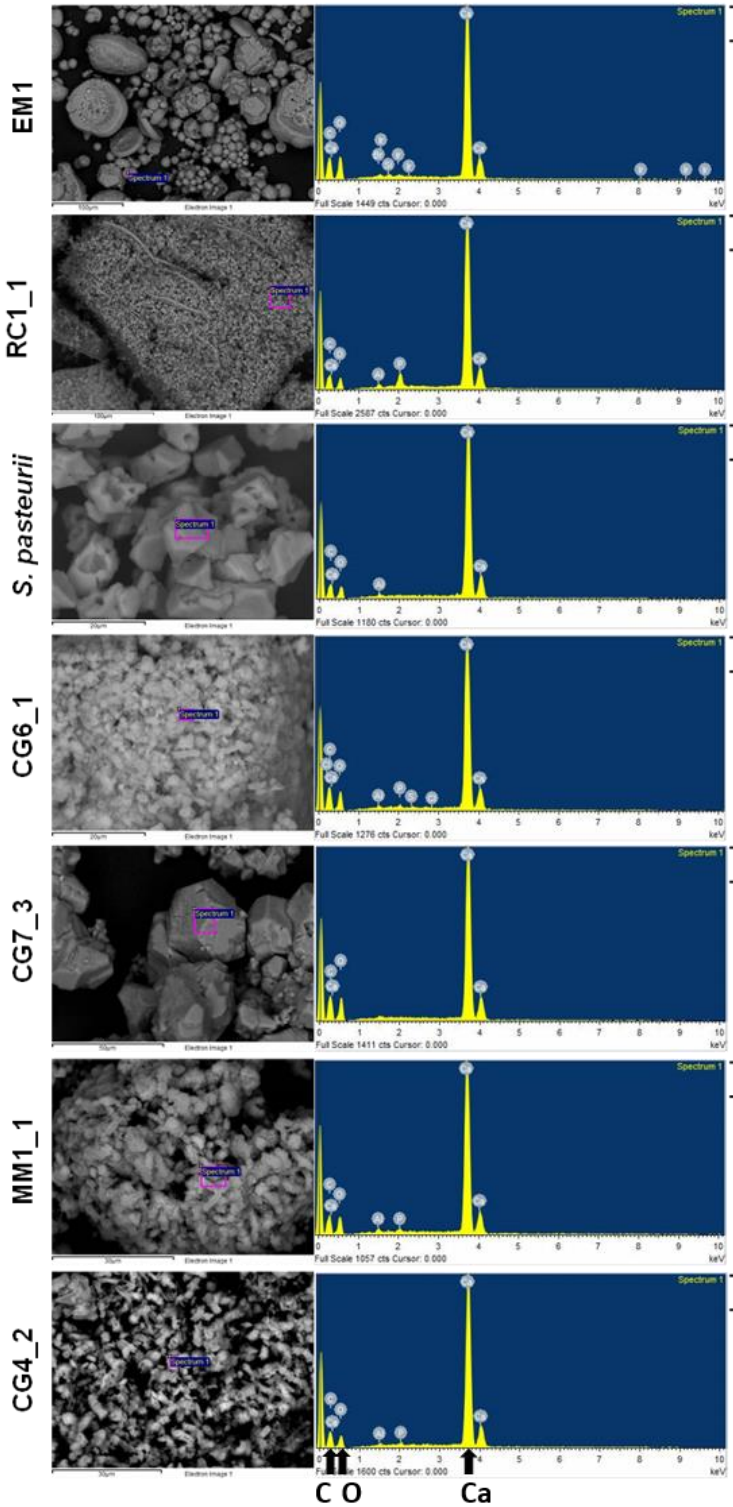

Element	Weight%	Atomic%
C	18.32	30.10
O	40.64	50.12
Ca	39.33	19.36
Totals	**98.29**	**99.58**

Element	Weight%	Atomic%
C	17.80	31.62
O	30.01	40.02
Ca	48.85	26.00
Totals	**96.66**	**97.64**

Element	Weight%	Atomic%
C	15.27	27.27
O	33.90	45.44
Ca	50.50	27.03
Totals	**99.67**	**99.74**

Element	Weight%	Atomic%
C	20.26	33.38
O	36.40	45.03
Ca	42.26	20.87
Totals	**98.92**	**99.28**

Element	Weight%	Atomic%
C	20.38	32.83
O	39.55	47.83
Ca	40.08	19.35
Totals	**100.00**	**100.00**

Element	Weight%	Atomic%
C	18.06	30.50
O	36.47	46.25
Ca	44.29	22.42
Totals	**98.82**	**99.17**

Element	Weight%	Atomic%
C	17.69	31.06
O	32.09	42.31
Ca	49.25	25.92
Totals	**99.03**	**99.29**

Figure S6. EDX analyses of precipitates produced by environmental bacteria. *Left,* the position on the precipitate where EDX was conducted (purple boxes). *Centre*, corresponding EDX spectra are shown, with the three peaks of main components labelled below. *Right,* elemental analysis indicating that the three main components (%) of the precipitate where carbon (C), oxygen (O), and calcium (Ca). Minor elements were excluded from the summary tables.

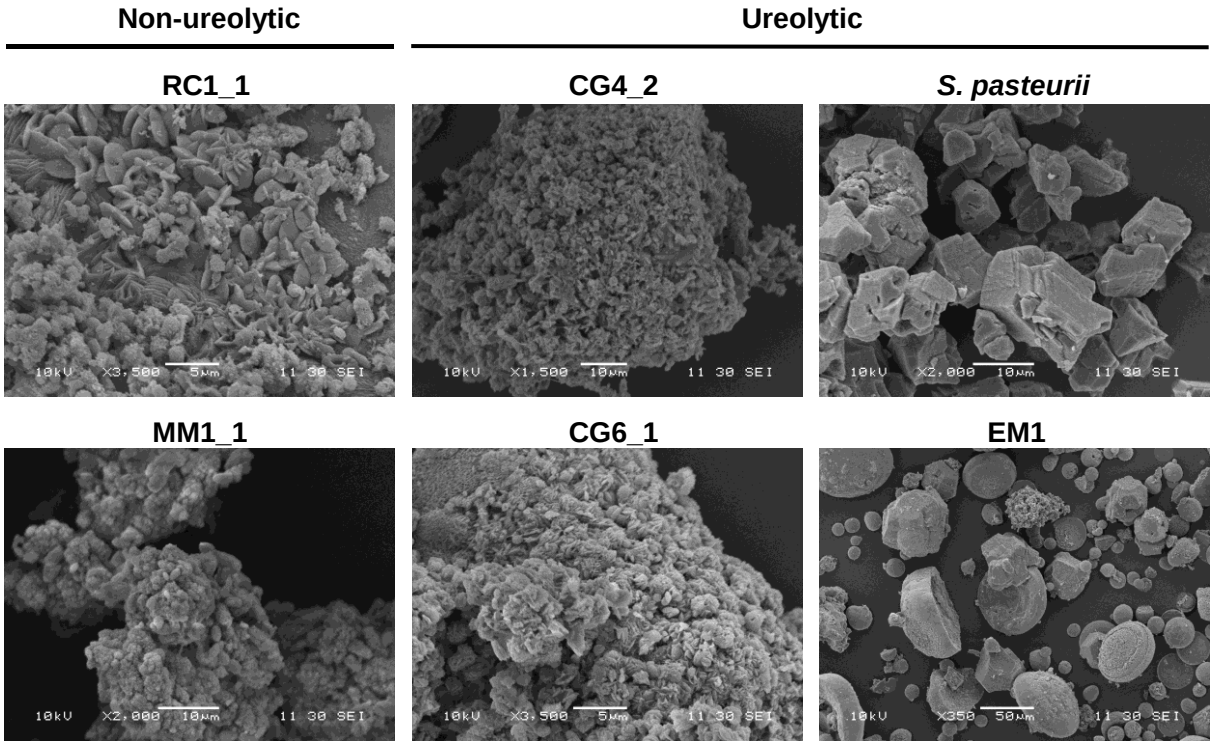

Figure S7. Crystal morphology in ureolytic and non-ureolytic isolates. Isolates were grown in LB medium supplemented with urea (20 g l^{-1}) and $Ca(OAc)_2$ (10 g l^{-1}) and electron micrographs of representative precipitates were taken between days 9-15. Strain names and their ureolytic potential are stated above.

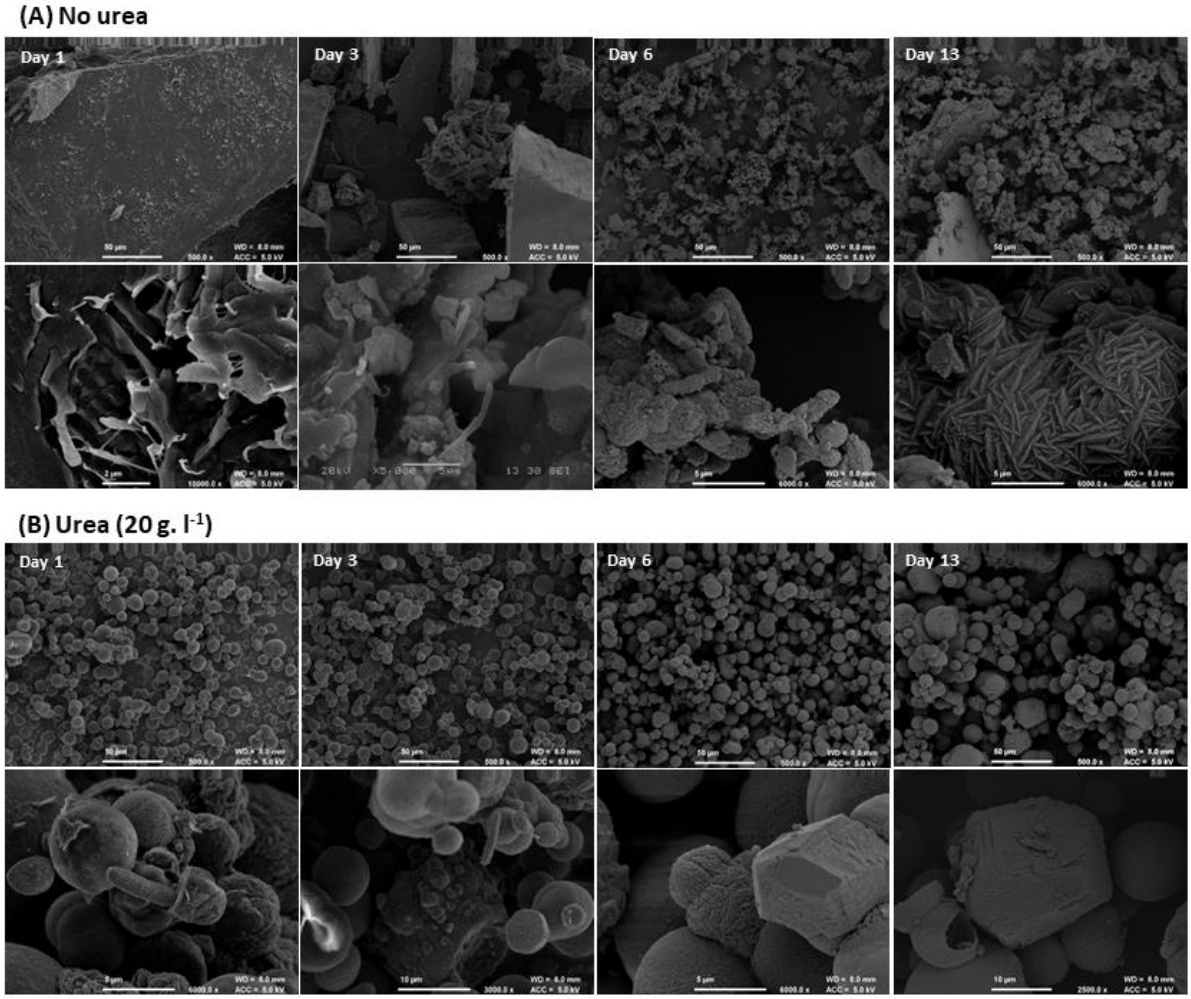

Figure S8. Comparison of crystal morphology in CG7_3 grown in the absence and presence of urea. The ureolytic strain CG7_3 was grown in LB medium supplemented with $Ca(OAc)_2$ (10 g l^{-1}) in the absence (A) and presence (B) of urea (20 g l^{-1}). Electron micrographs of precipitate were taken at days 1,3, 6 and 13. The top panel of each series represents a low magnification view, the bottom panel a high magnification close-up.

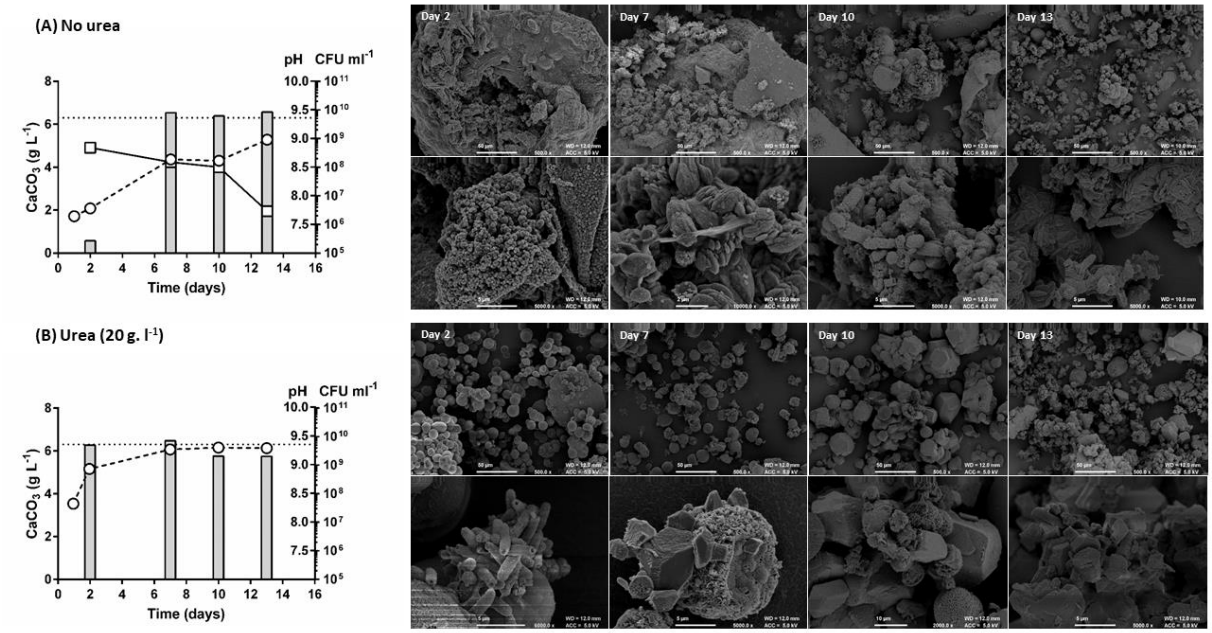

Figure S9. Comparison of ureolytic and non-ureolytic mechanisms of calcite precipitation in CG7_3. Ureolytic strain CG7_3 was grown in LB medium supplemented with $Ca(OAc)_2$ (10 g l^{-1}) in the absence (A) and presence (B) of urea (20 g l^{-1}). Precipitation of insoluble calcium carbonate (bars, g l^{-1}), pH changes (circles) and changes in cell number (boxes, CFU ml^{-1}) were monitored over time (days). *Right,* electron micrographs of representative precipitate taken at days 2, 7, 10 and 13.